Turnip yellow mosaic virus protease binds ubiquitin suboptimally to fine-tune its deubiquitinase activity

Sonia Fieulaine, Martin D Witte, Christopher S Theile, Maya Ayach, Hidde L Ploegh, Isabelle Jupin, Stéphane Bressanelli

Turnip yellow mosaic virus protease binds ubiquitin suboptimally to fine-tune its deubiquitinase activity

Received for publication, June 1, 2020, and in revised form, July 27, 2020 Published, Papers in Press, July 30, 2020, DOI 10.1074/jbc.RA120.014628

Sonia Fieulaine[1,*], Martin D. Witte[2], Christopher S. Theile[2], Maya Ayach[1], Hidde L. Ploegh[2], Isabelle Jupin[3], and Stéphane Bressanelli[1,*]

From the [1]Université Paris-Saclay, CEA, CNRS, Institute for Integrative Biology of the Cell (I2BC), 91198, Gif-sur-Yvette, France, the [2]Boston Children's Hospital and Harvard Medical School, Boston, Massachusetts, USA, and the [3]Laboratory of Molecular Virology, Jacques Monod Institute, CNRS, UMR, Université de Paris, Paris, France

Edited by Craig E. Cameron

Single-stranded, positive-sense RNA viruses assemble their replication complexes in infected cells from a multidomain replication polyprotein. This polyprotein usually contains at least one protease, the primary function of which is to process the polyprotein into mature proteins. Such proteases also may have other functions in the replication cycle. For instance, cysteine proteases (PRO) frequently double up as ubiquitin hydrolases (DUB), thus interfering with cellular processes critical for virus replication. We previously reported the crystal structures of such a PRO/DUB from *Turnip yellow mosaic virus* (*TYMV*) and of its complex with one of its PRO substrates. Here we report the crystal structure of TYMV PRO/DUB in complex with ubiquitin. We find that PRO/DUB recognizes ubiquitin in an unorthodox way: It interacts with the body of ubiquitin through a split recognition motif engaging both the major and the secondary recognition patches of ubiquitin (Ile^{44} patch and Ile^{36} patch, respectively, including Leu^{8}, which is part of the two patches). However, the contacts are suboptimal on both sides. Introducing a single-point mutation in TYMV PRO/DUB aimed at improving ubiquitin-binding led to a much more active DUB. Comparison with other PRO/DUBs from other viral families, particularly coronaviruses, suggests that low DUB activities of viral PRO/DUBs may generally be fine-tuned features of interaction with host factors.

Host–pathogen relationships are complex. The outcome of pathogen infection depends on a subtle balance between host immune responses triggered by infection and pathogen replication aimed at promoting propagation. In recent years, ubiquitination and deubiquitination events have emerged as central processes in antiviral mechanisms and viral multiplication (1–5). Ubiquitination is the conjugation of ubiquitin (Ub), a highly conserved 76-residue protein, to a target protein, through the formation of an isopeptide bond between the C-terminal glycine residue of Ub to a Lys of the target protein (6). Targets of ubiquitination are cellular proteins mostly involved in host immune responses and/or viral proteins (4). In certain cases, ubiquitin-like modifiers such as SUMO, NEDD8, or Ub-like ISG15 (interferon-simulated gene 15) may also be covalently attached to various substrates (7). Substrates are often polyubiquitinated, *i.e.* a chain of multiple Ub moieties, each linked by an isopeptide bond, is formed. Depending on the linkage type between distal and proximal Ub, the fate of tagged proteins varies, from targeting to proteasome or other degradation pathways for degradation (8) to nonproteolytic events such as interaction with various partners (6). Ubiquitination is a reversible process. Deubiquitination is catalyzed by deubiquitinases (DUBs), which can cleave isopeptide bonds to either trim, degrade, or edit polyUb chains from substrate proteins (7).

Because viruses strictly depend on the host to replicate and spread, they have evolved to circumvent or even hijack for their own advantage the ubiquitin-dependent responses triggered by entry of virus into the cell and subsequent replication (4, 9, 10). Indeed, a number of viruses have evolved DUBs (11, 12), either to counteract antiviral mechanisms or to favor their replication. The targets of viral DUBs can be cellular and/or viral proteins (11). As an example, deubiquitination of cellular proteins by viral DUBs can down-regulate the production of diverse antiviral molecules such as interferons or cytokines and allow viruses to evade host immune responses (12, 13). Another example is the deubiquitination of viral proteins by viral DUBs that avoids their targeting to the proteasome, a process that can be viewed as a rescue of these viral proteins. For some viruses an excess of certain viral proteins can be detrimental for viral replication (14, 15). These viruses use the deubiquitination step to modulate proteasome-dependent degradation to subtly control the level of the relevant proteins (9). For instance, adjusting the amount of RNA-dependent RNA polymerase (RdRp) may regulate the replication of some RNA viruses such as *Sindbis virus* (16), *Turnip yellow mosaic virus* (*TYMV*) (14, 17), or *Hepatitis A virus* (18).

DUBs are cysteine proteases or metalloproteases and are classified into seven families including two new families that have been recently defined (7, 19–21). These enzymes can specifically cleave one or several Ub linkage types or display a more general deubiquitinating activity. DUBs encoded by some single-stranded, positive-sense RNA viruses ((+)ssRNA viruses) such as arteriviruses, coronaviruses, picornaviruses, and tymoviruses are actually bifunctional enzymes also responsible for the viral polyprotein maturation through a protease (PRO) activity that cleaves defined peptide bonds (22–27). The molecular

This article contains supporting information.

*For correspondence: Sonia Fieulaine, sonia.fieulaine@i2bc.paris-saclay.fr; Stéphane Bressanelli, stephane.bressanelli@i2bc.paris-saclay.fr.

Present address for Martin D. Witte: Faculty of Science and Engineering, Chemical Biology 2, Stratingh Institute for Chemistry, Nijenborgh, Groningen, The Netherlands.

Present address for Christopher S. Theile: Alnylam Pharmaceuticals Inc., Cambridge, Massachusetts, USA.

determinants that regulate these dual activities remain largely unknown.

The dual PRO/DUB enzyme encoded by TYMV is a valuable example to address these questions because it is known to tightly regulate the level of RdRp during viral replication (24, 28). TYMV encodes an essential 206-kDa replicative polyprotein called 206K, which contains sequence domains indicative of methyltransferase (MT), PRO, NTPase/helicase (HEL), and RNA-dependent RNA polymerase (POL or RdRp) activities. The TYMV PRO domain first cleaves 206K to give rise to an intermediate product called 140K (encompassing the MT, PRO, and HEL domains) and the protein 66K (POL), after which it cleaves the 140K intermediate to release proteins called 98K (MT-PRO) and 42K (HEL) (29–31). The 66K polymerase is subject to phosphorylation and ubiquitination events triggered by the host, which ultimately target the modified protein to the proteasome where it is degraded (14, 32). Because of its DUB activity, the PRO domain of TYMV can counteract such degradation and inhibit 66K degradation (24). The whole process ensures a low level of 66K/POL in infected cells (33), the accumulation of which is deleterious for viral RNA replication (14). Although TYMV 66K is likely to be tagged with Lys^{48}-linked polyUb chains and TYMV PRO/DUB is able to process *in vitro* Lys^{48}- and Lys^{63}-linked polyUb chain (24), little is known about the type and the composition of polyUb chains attached to the 66K polymerase. In addition, how TYMV PRO/DUB recognizes ubiquitinated 66K is unknown.

The structure of TYMV PRO/DUB (34) has shown that the protein is a DUB from the ovarian tumor (OTU) family (7) that evolved to acquire a PRO function (34). Strikingly, *Tymoviridae* PRO/DUBs are the only OTU DUBs that lack two elements of the canonical cysteine protease active site displayed by all other OTU DUBs. First, it has only a catalytic dyad (composed of Cys^{783} and His^{869}) instead of the typical (Cys-His-Asp/Asn) triad of OTU DUBs. The Asp/Asn residue is replaced by a serine (Ser^{871} in TYMV PRO/DUB) that is conserved in the other members of the *Tymoviridae* family (34). Second, there is no pocket that could constitute the oxyanion hole that is formed during the catalytic mechanism (34). In contrast, *Tymoviridae* PRO/DUBs display a unique loop (Gly^{865}-Pro^{866}-Pro^{867}) in close vicinity of the active site (34). We previously concluded that this loop is involved in substrate recognition and contributes to align the side chains of catalytic residues (28). The mobility of this loop therefore would contribute to switching from the PRO activity to the DUB activity. In one of the TYMV PRO/DUB crystal structures, the protein has adventitiously self-assembled into the active form (35), leading to a physiologically relevant PRO/DUB·PRO complex[4] that gives clues to the mechanism of the PRO function of the enzyme. Indeed, this structure provides a snapshot of how the enzyme recognizes the C-terminal extremity of another PRO domain during the PRO↓HEL cleavage event, which occurs in the course of polyprotein maturation (30, 34).

To better understand the DUB function of the TYMV PRO/DUB domain, we report its crystal structure in complex with ubiquitin. We supplemented the low resolution of the structure (3.7 Å) with molecular dynamics simulations. We used this modeling approach to further probe the differences in molecular recognition between two of its substrates, *i.e.* PRO of the PRO↓HEL cleavage site and ubiquitin. A structure-guided mutagenesis study identified point mutants with an increased DUB activity, showing that the unusual recognition of Ub by TYMV PRO/DUB is suboptimal. Comparison of this PRO/DUB–Ub structure with that of the PRO/DUB·PRO complex that occurs during polyprotein processing (34) shows that these unrelated substrates are recognized by largely overlapping recognition surfaces.

Results

Overall structure of the covalent TYMV PRO–Ub complex

To solve the crystal structure of a TYMV PRO/DUB·ubiquitin complex and because the affinity of a single module of Ub for the enzyme is low (24, 34), we used a modified form of Ub (Ub-VME) in which the C-terminal Gly^{76} is substituted with a vinyl methylester function that spontaneously and irreversibly forms a covalent linkage with the catalytic cysteine of DUBs in a Michael addition (36, 37). TYMV PRO/DUB and Ub-VME were incubated at 25 °C, leading to the formation of a covalent complex as evidenced by SDS-PAGE (Fig. S1*A*), which was then purified by size-exclusion chromatography (Fig. S1*B*). Crystals of the protein complex grew in a single drop after 120 days. Only a single crystal showed acceptable diffraction that allowed us to collect data. The structure was solved at 3.7 Å resolution by molecular replacement. The crystallographic asymmetric unit contains two PRO/DUB–Ub complexes, one of which is well-ordered and could be modeled with confidence, except in a few places where density was ambiguous. We complemented this crystallographic model with molecular dynamics simulations that helped to resolve ambiguities and allowed an accurate view of the complex (see below for details). The second complex in the asymmetric unit was modeled from the first and the structure refined with tight noncrystallographic restraints with good statistics (Table 1). We will limit our analysis to the single well-ordered complex composed of chains A (TYMV PRO/DUB, ordered residues 732–876 by polyprotein numbering) and B (Ub-VME, residues 1–76 including the terminal glycyl-vinylmethylester covalently linked to the catalytic Cys^{783}).

The interaction surface of the PRO/DUB–Ub complex measured by PISA server (38) buries 860 $Å^2$ (11%) and 908 $Å^2$ (19.5%) of solvent-accessible area for the TYMV PRO/DUB and Ub molecules, respectively, which is on the lower side of the reported values for other DUB·Ub complexes (39–41). As in these other complexes, the Ub-binding interface of TYMV PRO/DUB can be viewed as two distinct areas (Fig. 1). First, the body of Ub is bound by a surface of TYMV PRO/DUB distant from the PRO/DUB active site and contributed on one side by its N-terminal lobe (residues 732–770) and on the other by the C-terminal lobe (residues 836–876; for a more detailed description of the three lobes, see Ref. 34). Second, the C-terminal extremity of Ub inserts into the TYMV PRO/DUB catalytic cleft between the central lobe (residues 773–835) and the C-terminal lobe.

[4] The character "·" is used for a noncovalent complex (PRO/DUB·PRO), and "–" indicates a covalent complex (PRO/DUB–Ub).

Table 1
Data collection and refinement statistics
Statistics for the highest-resolution shell are shown in parentheses.

Data collection	
Wavelength (Å)	0.978
Space group	P 1 21 1
Unit cell (Å, °)	37.93, 51.86, 125.25, 90, 98.37, 90
Resolution range	37.46–3.679 (3.81–3.679)
Total reflections	17,522
Unique reflections	5,303
Multiplicity	3.3 (3.3)
Completeness (%)	97.96 (85.85)
Mean I/sigma(I)	4.14 (0.97)
Wilson B-factor	106.81
R_{merge}	0.215 (1.211)
$CC_{1/2}$	98.5 (41.5)
Refinement	
Reflections used in refinement	5,290 (467)
Reflections used for R_{free}	265 (24)
R_{work}	0.2057 (0.3269)
R_{free}	0.2837 (0.3611)
Root-mean-square deviation	
Bonds	0.004
Angles	0.51
Ramachandran (%)	
Favored	92.13
Allowed	7.87
Outliers	0.00
Rotamer outliers (%)	3.00
Clashscore	7.30
Average B-factor	175.69
Macromolecules	175.62
Ligands	190.88
Number of TLS groups	4

TYMV PRO/DUB uses two polar loops to simultaneously engage the two major hydrophobic patches on the body of Ub

Distant from the active site, the interaction of TYMV PRO/DUB with Ub appears quite unusual: Ub plugs into a large groove at the surface of TYMV PRO/DUB, so that both of its major recognition patches (the so-called Ile^{44} and Ile^{36} patches) are bound simultaneously (Fig. 1*A*). On one side of the groove, the Ile^{44} patch is contacted by the *Tymoviridae*-specific N-terminal lobe (residues 732–772), whereas on the other side, the Ile^{36} patch is contacted by the C-terminal lobe that is common to all OTU DUBs.

The Ile^{44} patch-interacting site

The side chains of TYMV PRO/DUB Glu^{759} and Asn^{760}, from the N-terminal lobe of the protein, project directly toward the Ile^{44} patch of Ub, composed of residues Ile^{44}, Leu^{8}, His^{68}, and Val^{70} (6) (Fig. 2*A*). In previous work based on a docking model of the complex and a subsequent mutagenesis study, we suspected the involvement of Glu^{759} and Asn^{760} in Ub recognition. We hypothesized the presence of a hydrogen bond between Asn^{760} and His^{68} and a salt bridge between Glu^{759} and Lys^{6} and/or His^{68} (34). Indeed the simultaneous replacement of these two residues by two Gly residues (mutation E759G/N760G) led to a small but significant decrease of DUB activity *in vitro* (34). No such interactions are seen in the crystal structure (Fig. 2*A*). However, Lys^{6} of Ub is engaged in a strong crystal contact with Asp^{739} and Thr^{741} from a neighboring molecule

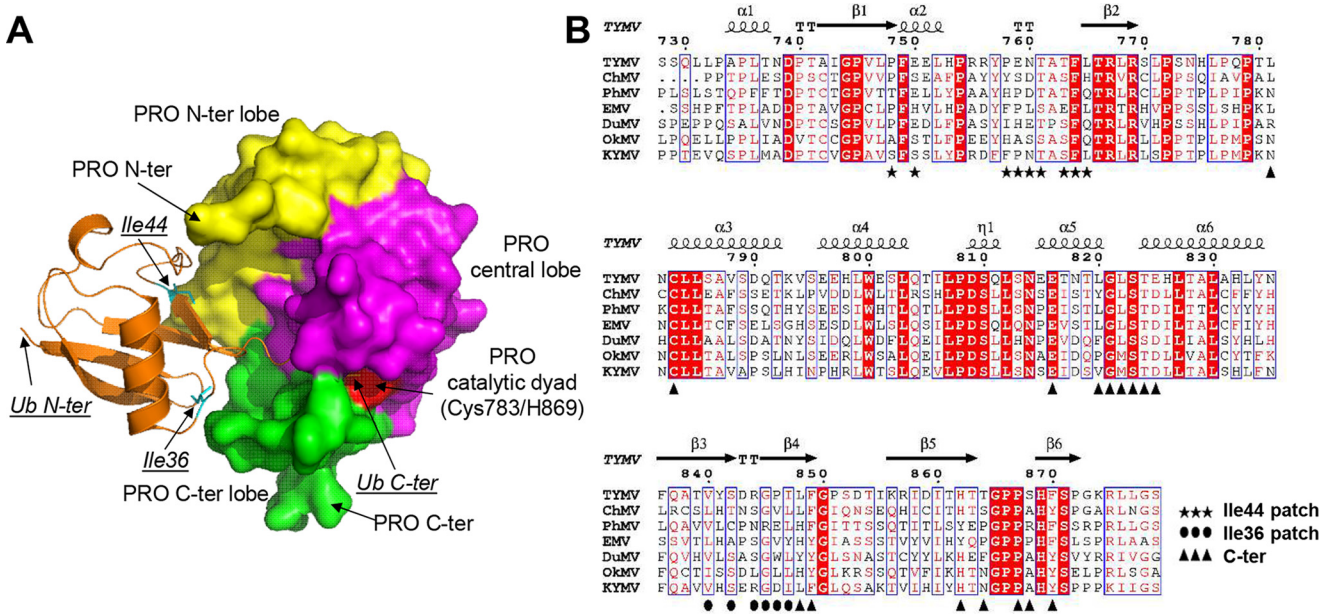

Figure 1. Overall structure of the covalent TYMV PRO/DUB–Ub complex. *A*, crystal structure of the covalent TYMV PRO/DUB–Ub complex. TYMV PRO/DUB is represented as molecular surface, with the N-terminal (*N-ter*) lobe in *yellow*, the central lobe in *magenta*, and the C-terminal (*C-ter*) lobe in *green*. The enzyme's catalytic dyad, composed of Cys^{783} and His^{869}, is indicated in *red*. HA–Ub-VME is shown in ribbon diagram and colored in *orange*. Residues Ile^{36} and Ile^{44} are displayed in ball-and-stick format and colored in *cyan*. Ubiquitin residues are labeled in *italics* and *underlined*. *B*, sequence alignment of polyprotein processing endopeptidases belonging to the *Tymoviridae* family. The sequence of TYMV PRO/DUB was aligned with enzymes encoded by *Chayote mosaic virus* (*ChMV*), *Physalis mottle virus* (*PhMV*), *Eggplant mosaic virus* (*EMV*), *Dulcamara mottle virus* (*DuMV*), *Okra mosaic virus* (*OkMV*), and *Kennedya yellow mosaic virus* (*KYMV*) as in the work of Lombardi *et al.* (34). Alignment was performed by CLUSTALW (82), edited, and displayed with ESPript3 (83). *White characters* in *red boxes* indicate identity, and *red characters* in *white boxes* indicate homologous residues. Secondary structures of TYMV PRO/DUB (PDB code 4A5U (34)) are indicated on *top*. *Black stars* indicate the residues of enzyme interacting with Ub Ile^{44} hydrophobic patch, *black circles* indicate the residues interacting with Ub Ile^{36} hydrophobic patch, and *black triangles* indicate the residues interacting with the C-ter extremity of Ub.

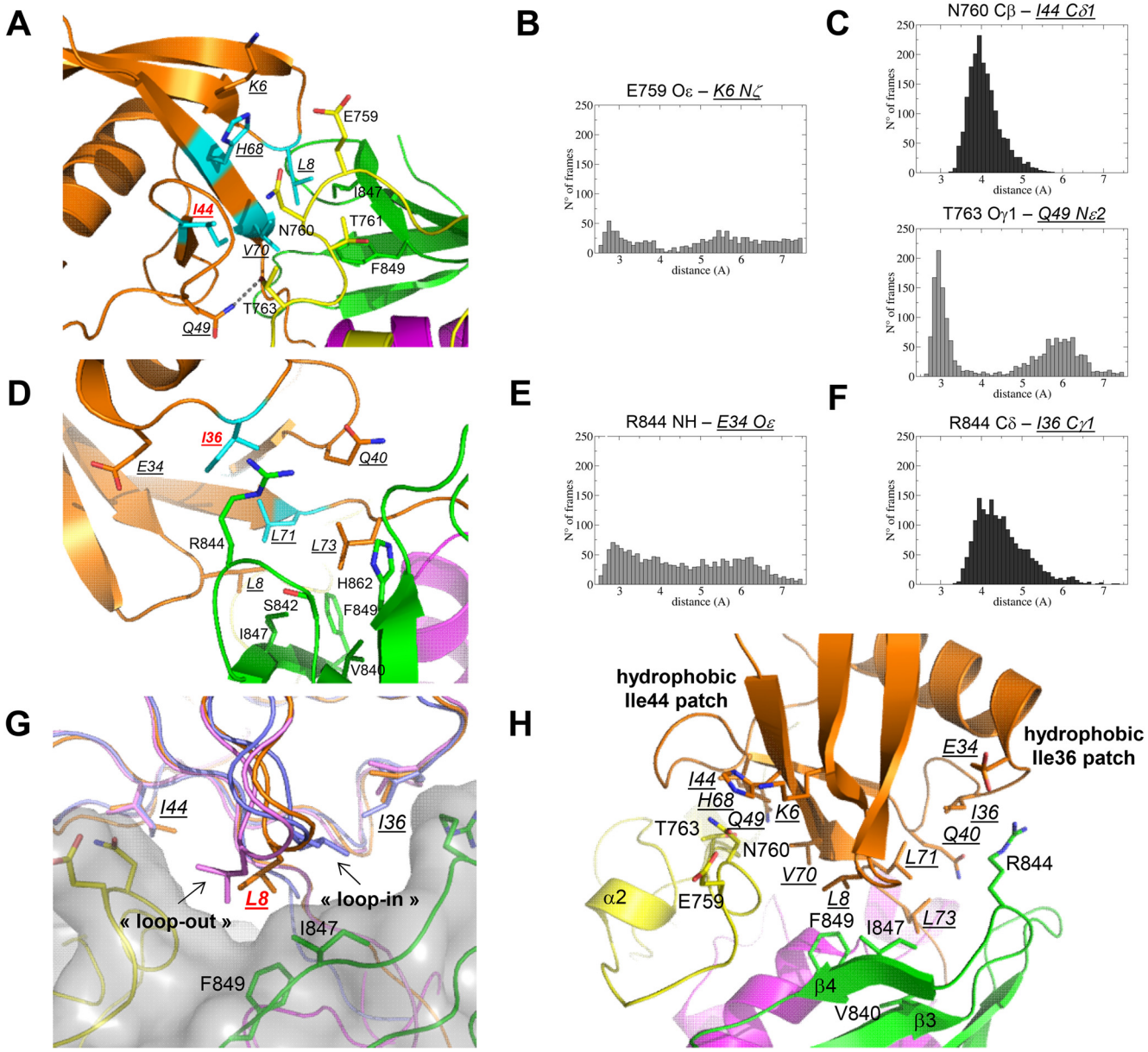

Figure 2. Interactions between TYMV PRO/DUB and Ub. *A*, close-up view of the Ub Ile^{44} patch. Both proteins are shown in cartoon, and residues involved in the interaction are shown in stick. Proteins are colored as in Fig. 1, with oxygen and nitrogen atoms in *red* and *blue*, respectively. The hydrogen bond between Gln^{49} from Ub and Thr^{763} from TYMV PRO/DUB is shows as a *dotted line*. *B* and *C*, analysis of interactions around the Ub Ile^{44} patch by molecular dynamics simulations. The distances between three pairs of residues were measured during 90 ns of production time in two simulations, and their frequency was plotted. *Gray*, hydrogen bonds and electrostatic interactions; *black*, hydrophobic contact. *D*, close-up view of the Ub Ile^{36} patch. Proteins and residues are represented and colored as in *A*. *E* and *F*, analysis of interactions around the Ub Ile^{36} patch by molecular dynamics simulations. The distances between two pairs of residues were measured during 90 ns of production time in two simulations, and their frequency was plotted, as in *B* and *C*. *G*, close-up view around Leu^{8} of Ub. Both proteins are displayed in cartoon loop with some side chains shown in stick. The cavity of TYMV PRO/DUB that fits Ub is highlighted by the *gray molecular surface* of the enzyme. Three crystal structures of Ub were superimposed to compare the position of the loop encompassing Leu^{8}: *purple*, loop-out conformation (PDB code 1UBQ (73)); *orange*, intermediate conformation (this work); *blue*, loop-in conformation (PDB code 2G45 (84)). *H*, overall view of the two polar loops of TYMV PRO/DUB that bind the two hydrophobic patches of Ub.

(data not shown). This precludes any interaction with TYMV PRO/DUB in the asymmetric unit but does not exclude the existence of such an interaction in solution. Hence, to better understand the interaction network between TYMV PRO/DUB Glu^{759} and Asn^{760} residues and the Ile^{44} patch of Ub, we performed molecular dynamics simulations of the complex. For the starting model, we made two changes that depart from the crystal structure: we first replaced the C-terminal ubiquitin residue (a Gly substituted with a vinyl methylester group; see above) with an unmodified glycine. Thus, the complexes we simulated mimicked product-bound states, as in our previous structure of a PRO/DUB·PRO complex (34). Second, we modeled residues 727–731 that are not visible in the electron density map, and we acetylated Ser^{727} to better model the native state of the TYMV PRO/DUB domain (that is, linked to the rest of the polyprotein by its N terminus). When free from crystal contacts, Lys^{6} now points toward the side chain of Glu^{759}. However, in two independent 50-ns simulations, the two

residues never engaged in the formation of a stable salt bridge. This is readily shown by the distribution of distances between atom Nζ of Lys^{6} and atom Oϵ of Glu^{759}, which shows only a minor peak at 2.8 Å (Fig. 2*B*). Instead the simulations confirm a strong involvement in the interface of the aliphatic portions of the Glu^{759}, Asn^{760}, Thr^{761}, and Thr^{763} side chains. They pack against the hydrophobic Ile^{44} patch of Ub (Fig. 2*C*, *top panel*). The only polar interaction between these polar residues and ubiquitin is a hydrogen bond between Thr^{763} and Gln^{49} (~50% occupancy) (Fig. 2*C*, *bottom panel*).

Although our previous docked model of the TYMV PRO/DUB·Ub complex suggested the potential involvement of another part of the N-terminal lobe (including Leu^{732} and Leu^{765}) in Ub binding (34), the crystal structure now shows these residues lying at the edge of the Ile^{44} patch in the vicinity of Ub residues Gln^{49}, Glu^{51}, and Asp^{52} (Fig. S2) and with, at best, a small contribution to the interface. Simulations consistently show that Leu^{732} and Leu^{765} actually tend to come away from ubiquitin (data not shown). This is in agreement with our previous report that Ala mutations of these residues (mutation L732A/L765A) showed no effect on DUB activity *in vitro* (34), ruling out their involvement in Ub binding.

The Ile^{36}-interacting site

The Ile^{36} patch of Ub, the core of which is composed of residues Ile^{36} and Leu^{71} (6), is positioned against segment 840–847 of TYMV PRO/DUB (Fig. 2*D*), with Ile^{847} also interacting with Ub Leu^{8} (see below). Arg^{844} is clearly the TYMV PRO/DUB residue closest to Ile^{36}, but density for the side chain of Arg^{844} fades beyond its Cγ. Thus, to obtain a better view of the Arg^{844} side chain, we analyzed its behavior in molecular dynamics simulations. The simulations show that the charged end of the Arg^{844} side chain is highly mobile and samples a large conformational space, where it finds several defined bound states. Indeed, guanidinium function of Arg^{844} alternatively makes a transient salt bridge with the Ub Glu^{34} side chain (Fig. 2*E*) or hydrogen bonds with the Ub Gln^{40} side-chain or main-chain carbonyls of Ub Glu^{34} and Gly^{35} (data not shown). In contrast, the aliphatic portion of Arg^{844} down to Cγ remains stably packed against the Ub Ile^{36} patch (Fig. 2*F*). Thus, we arrived at a similar picture as for the region of the Ub Ile^{44} patch, with polar or charged residues of TYMV PRO/DUB contacting the hydrophobic patches of Ub almost exclusively by their aliphatic portions.

The Leu^{8}-interacting site

Leu^{8} of Ub is located between the two hydrophobic patches, in a flexible loop that connects the two first α-helices (42, 43). This loop can undergo conformational changes, from a "loop-out" to a "loop-in" position (44), which in turn enables it to be part of either the Ile^{44} or the Ile^{36} patch (44, 45) (Fig. 2*G*). The flexibility of the loop that comprises Leu^{8} is now recognized to be important for recognition of ubiquitin-binding proteins (UBPs) (43). In the TYMV PRO/DUB–Ub complex, this loop adopts an intermediate position between the loop-out and loop-in positions, and Leu^{8} points toward the bottom of the groove (Fig. 2*G*). In this region, Ile^{847} and Phe^{849} of TYMV PRO/DUB make strong hydrophobic contacts with Leu^{8}, Thr^{9}, Val^{70}, Leu^{71}, and Leu^{73} of Ub. This centrality of Ile^{847} in an interaction network based essentially on hydrophobic interactions is consistent with our previous work. Indeed, mutating Ile^{847} to Ala, which conserves its apolar properties, has a significant but mild effect on DUB activity, both *in vitro* and *in vivo*, whereas addition of a negative charge in this region (mutation I847D) drastically decreased DUB activity (28, 34).

In summary, the crystal structure of the covalent complex between TYMV PRO/DUB and Ub, supplemented by molecular dynamics simulations, shows that Ub nestles in a cavity of TYMV PRO/DUB. This binding mode mimics a clamp that holds Ub through hydrophobic interactions made, surprisingly, by TYMV PRO/DUB polar and charged residues, with one side of the clamp formed by the α2-β2 loop containing the Pro^{758}-Glu^{759}-Asn^{760}-Thr^{761}-Ala^{762}-Thr^{763} motif and the other side of the clamp constituted essentially by residues belonging to β3 and β4 strands, centering on Arg^{844} in the β3-β4 loop (Figs. 1*B* and 2*H*). The bottom of the Ub-binding groove is composed of hydrophobic residues that are part of β-strands β3 and β4. On its side, Ub engages three binding sites simultaneously, *i.e.* in addition to its C terminus (see below): the two hydrophobic patches centered on Ile^{44} and Ile^{36} connected by the loop encompassing Leu^{8}. Despite this three-part contact, the buried surface is on the small side compared with other viral DUB·Ub complexes.

TYMV DUB activity can be improved by point mutations that affect the atypical binding surface used to contact Ub

To probe the puzzling use of polar residues in TYMV PRO/DUB to bind the Ub hydrophobic patches and determine the relative contributions of polar and hydrophobic contacts, we produced and assayed several structure-guided point mutants for DUB activity. The activity of the mutant proteins produced in *Escherichia coli* was measured using the general DUB substrate ubiquitin-7-amino-4-methyl coumarin (Ub-AMC) as described (24, 34). In this *in vitro* test, TYMV PRO/DUB is not saturated, even at the highest Ub-AMC concentrations attainable (34). It is therefore not possible to determine precisely the k_{cat} and K_m parameters. Instead, the assay far from saturation allows the measurement of K_{app} that approximates k_{cat}/K_m. First, we mutated polar residues that interact with the Ile^{44} hydrophobic patch of Ub. Replacement of Glu^{759} or Asn^{760} by alanine resulted in substantially increased DUB activity compared with the WT enzyme: 137 ± 7% and 135 ± 8% for E759A and N760A, respectively (Fig. 3*A*). The charged carboxylate of Glu^{759} is thus actually detrimental to DUB activity. This is consistent with structural data that highlight the importance of the apolar portions of the interfacial residues and the flickering nature of polar interactions, such as the Glu^{759}–Lys^{6} salt bridge. Finally, DUB activity can actually be increased by the removal of polar groups and maintaining only apolar side chains. In contrast, mutation of Thr^{763} to alanine showed a slightly decreased DUB activity (89 ± 8%; see Fig. 1*G*), again in accordance with structural and sequence data (Figs. 1*B* and 2*C*, *bottom panel*).

Second, we wanted to better understand the role of Arg^{844} side chain, which can not only make van der Waals contacts with the Ile^{36} hydrophobic patch of Ub but also can form

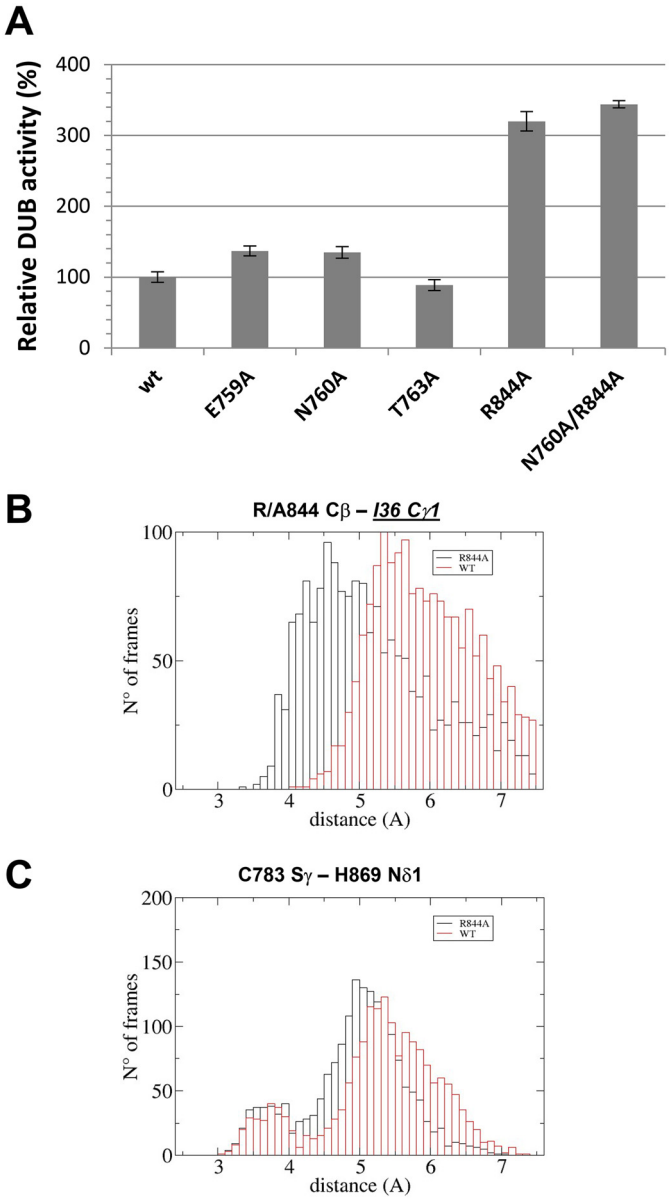

Figure 3. *In vitro* DUB activity of structure-guided mutants of TYMV PRO/DUB. *A*, DUB activity of recombinant TYMV PRO/DUB (WT and structure-guided mutants) was measured by a fluorescence assay using Ub-AMC as substrate. K_{app} was determined according to the equation $V/[E] = K_{app}[S]$, where V is the initial velocity calculated from the kinetic data, and [E] and [S] are the corresponding enzyme and substrate concentrations. The values are expressed as the percentages of that of WT protein. *B* and *C*, behavior of residue 844 side chain (*B*) and of the catalytic dyad (Cys^{783} and His^{869}) (*C*) was investigated by performing molecular dynamics simulations of the product state complex, using WT TYMV PRO/DUB or R844A mutant. The R844A mutant was generated by truncating the Arg side chain at Cβ to mimic an alanine. The distances were measured along the same 90 ns in two simulations as in Fig. 2 (WT, *red histograms*) and along 90 ns in two simulations for R844A (*black histograms*). *B*, distance between the side chains of TYMV PRO/DUB residue 844 (Cβ atom) and Ub Ile^{36} (Cγ1 atom). *C*, distance between TYMV PRO/DUB Cys^{783} (Sγ atom) and His^{869} (Nδ1 atom). The minor peak at 3.5 Å signals alignment of the catalytic dyad.

hydrogen bonds or a salt bridge with several Ub residues (Fig. 2*E*). We thus replaced Arg^{844} by Ala. This mutation led to a dramatic 3-fold increase of DUB activity (320 ± 14%; see Fig. 3*A*), an effect also observed with the double mutant N760A/R844A (344 ± 5%; see Fig. 3*A*). This implies that Arg at position 844 of TYMV PRO/DUB is detrimental to DUB activity. Because this residue is located far away from the active site, it is likely that its polar side chain alters the binding to Ub rather than affects the turnover of the enzyme. The observation that TYMV DUB activity can be substantially improved by point mutations prompted us to model the interaction of the R844A mutant with Ub. We performed molecular dynamics simulations of the complex in the same conditions as for the WT and with the same initial models, albeit with the truncation of the Arg^{844} side chain to mimic an alanine. In two independent replicates the complex shifted from its initial conformation to one in which Ala^{844} packs against the center of the Ile^{36} patch, as exemplified by the new van der Waals contacts of Ala^{844} Cβ with Ile^{36} Cγ1 (Fig. 3*B*). In contrast, the catalytic dyad's dynamics were not affected, as shown by the continued rarity of the activating hydrogen bond between His^{869} and Cys^{783} (Fig. 3*C*). These results show how the complex can easily adjust to the much smaller alanine side chain to effectively shield the Ile^{36} patch from solvent, without disturbing the active site. They confirm the centrality of the apolar contact between residue 844 and Ub and suggest that the effect of R844A is indeed on ubiquitin binding rather than on enzyme turnover.

Altogether, these results reinforce the conclusion that TYMV PRO/DUB indeed binds both Ile^{44} and Ile^{36} patches of Ub suboptimally, contributing to a poor DUB activity. They establish that point mutations aimed at improving Ub binding do result in a considerably increased DUB activity.

Binding mode of the C-terminal tail of Ub: how TYMV PRO/DUB recognizes different C-terminal sequences

In addition to interactions that involve the body of Ub via its two conserved hydrophobic patches, a large portion of PRO/DUB·Ub interacting surface engages the five C-terminal residues of Ub inserted into the catalytic cleft of TYMV PRO/DUB (Fig. 1*A*). As expected, the C-terminal tail of Ub adopts a β conformation that creates a dense hydrogen-bonding network with TYMV PRO/DUB residues that belong to the substrate-binding site (Fig. 1*B*). These involve the backbone carbonyl oxygens and amide hydrogens of Leu^{822}, Thr^{824}, and Ser^{868}, and side chains of Thr^{824} and Ser^{868} (Fig. 4*A*). The strong electron density in the vicinity of Arg^{74} of Ub was difficult to interpret at this resolution, because the side chains of Arg^{72} and Arg^{42} also point in the same direction. Again, molecular dynamics simulations were helpful in settling this ambiguity. Only the Cβ of the three arginines were initially modeled in the crystal structure. Alternate solutions for their side chains were then generated, all consistent with electron density, and simulations were performed. Simulations nicely converged to the same arrangement in that region, no matter the starting point. We kept this solution for refinement of the crystal structure (Fig. 4*B*). The three arginines all point toward the acidic S5 pocket of TYMV PRO/DUB, comprised of Glu^{816} and Glu^{825} (34). Arg^{72} and Arg^{74} of Ub both make salt bridges with Glu^{816} and/or Glu^{825}, a type of interaction often seen in other complexes involving Ub (37, 40, 41, 46–49). The side chain of Asp^{39} from Ub also points toward Arg^{74} (the two make a stable salt bridge in the simulations), making a ring of acidic residues around the three clustered arginines (Fig. 4*B*).

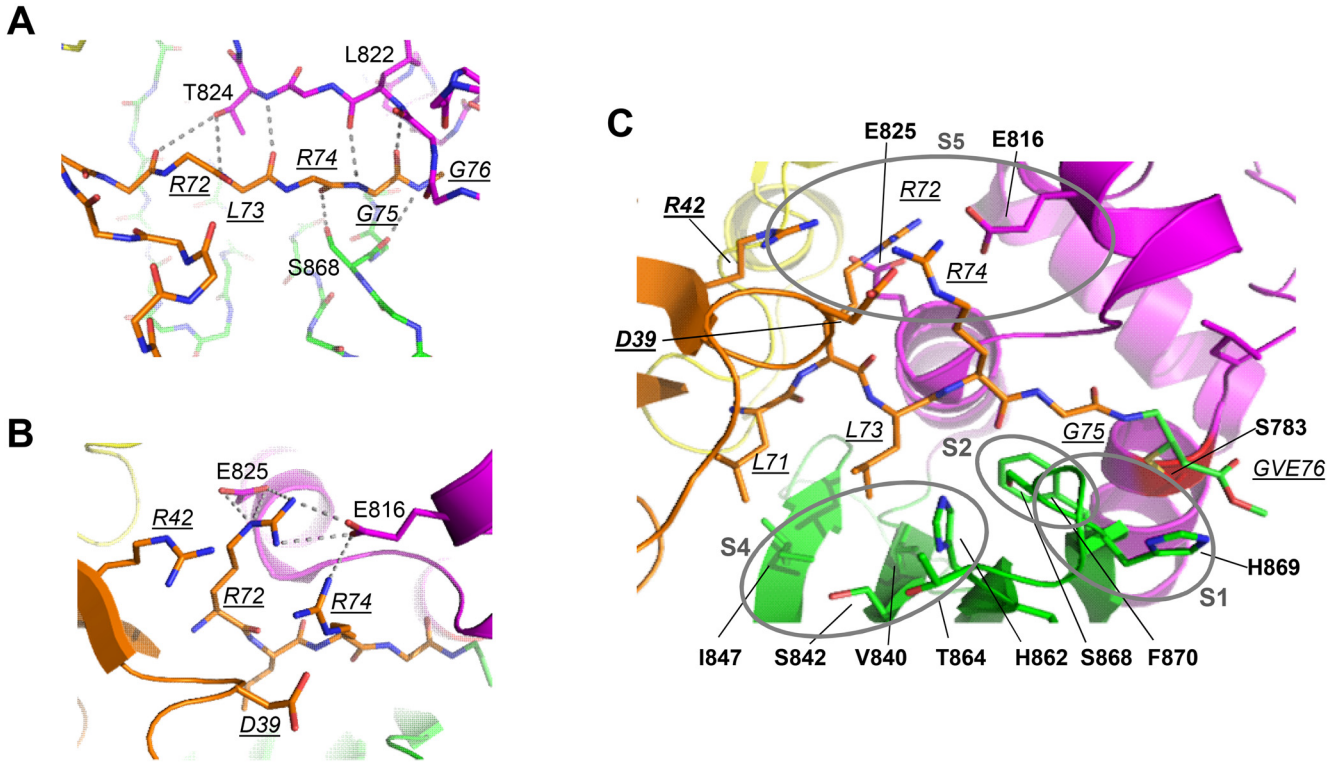

Figure 4. Interactions network at the C-terminal tail of Ub. *A*, detailed hydrogen bonding between the last five residues of Ub and TYMV PRO/DUB. The C-terminal extremity backbone of Ub (including Arg^{72} to Gly-VME76) is represented as sticks. The residues of TYMV PRO/DUB involved in the interaction with Ub are displayed as sticks. Hydrogen bonds are shown as *dotted lines*. *B*, electrostatic interactions between three Arg of Ub (Arg^{42}, Arg^{72}, and Arg^{74}) with the acidic pocket of TYMV PRO/DUB constituted by Glu^{816} and Glu^{825}, and Asp^{39}.*C*, global hydrophobic interactions network between the last five residues of Ub and TYMV PRO/DUB. Both proteins are shown in cartoon, with residues involved in interaction depicted in sticks. The overall coloring scheme is the same as that in Figs. 1 and 2.

We can now assess how the PRO/DUB catalytic cleft adjusts to different substrates. Indeed, TYMV PRO/DUB recognizes a consensus peptide substrate (K/R)L*X*G(G/A/S) (corresponding to positions P5-P4-P3-P2-P1), where *X* is any amino acid, corresponding to the HEL↓POL and PRO↓HEL cleavage sites (KLNGA↓ and RLLGS↓, respectively) and the C-terminal extremity of Ub (RLRGG↓). The requirements for this sequence can be explained by a comparison of the crystal structure of TYMV PRO/DUB–Ub complex with that of the PRO/DUB·–PRO complex with the C-terminal extremity of a PRO from PRO↓HEL cleavage site inserted in the catalytic cleft of a PRO enzyme (see Fig. 3 in Ref. 34). Overall, the acidic S5 pocket of TYMV PRO/DUB, composed of residues Glu^{816} and Glu^{825}, highly conserved in the *Tymoviridae* family (see sequence alignment in Fig. 1*B*), always accommodates a basic residue at position P5 (Lys or Arg, see above). In the specific case of Ub, the combination of the TYMV PRO/DUB acidic patch and an acidic residue from Ub (Asp^{39}) perfectly accommodate the three Arg of Ub, two belonging to its C terminus (Arg^{72} and Arg^{74}) and one oriented toward its C terminus (Arg^{42}). The strict requirement for a Leu at position P4 is imposed by the hydrophobic S4 pocket, created by residues Val^{840}, Ser^{842}, Ile^{847}, and His^{862} (Fig. 4*C*) rather conserved in homologous PROs (Fig. 1*B*). The absence of a real S3 pocket leads to a relaxed specificity at the P3 position, accommodating structurally unrelated residues such as Arg, Leu, or Asn. The conserved Gly at position P2 fits in a pocket containing Ser^{868} and Phe^{870}. These two residues, conserved in the *Tymoviridae* family (Fig. 1*B*), constitute the so-called glycine specificity motif, a common feature of alphavirus PROs and PRO/DUBs (50, 51). Finally, limited specificity for a small side chain at position P1 is due to the flexible enzyme's Thr^{864}-Gly^{865}-Pro^{866}-Pro^{867}-Ser^{868} loop, which regulates the constriction of the S1 pocket and consequently substrate specificity and enzymatic activity (28). The GPP motif is a strictly conserved (Fig. 1*B*) addition to the OTU DUB fold found in the *Tymoviridae* family.

In conclusion, the C-terminal residues of Ub assume an extended conformation and occupy the catalytic cleft of TYMV PRO/DUB. They do so by creating an intricate network of salt bridges, further strengthened by numerous hydrophobic contacts. The consensus sequence of the C-terminal extremity of PRO, HEL, and Ub, composed of invariant residues (positions P4 and P2), conserved residues (positions P5 and P1) and nonconserved residues (position P3), eventually defines which residues are specificity determinants. These allow TYMV PRO/DUB to discriminate among its substrates. The TYMV PRO/DUB is actually a deubiquitinase that acquired a protease function to process its polyprotein (34) (see also "Discussion"). It is likely that the PRO's substrate cleavage sites have evolved to mimic the C-terminal extremity of Ub. Such optimization of substrate sequences allows a single enzyme to perform several enzymatic reactions. Although this may be a simplification, it supports the "genetic economy" concept that

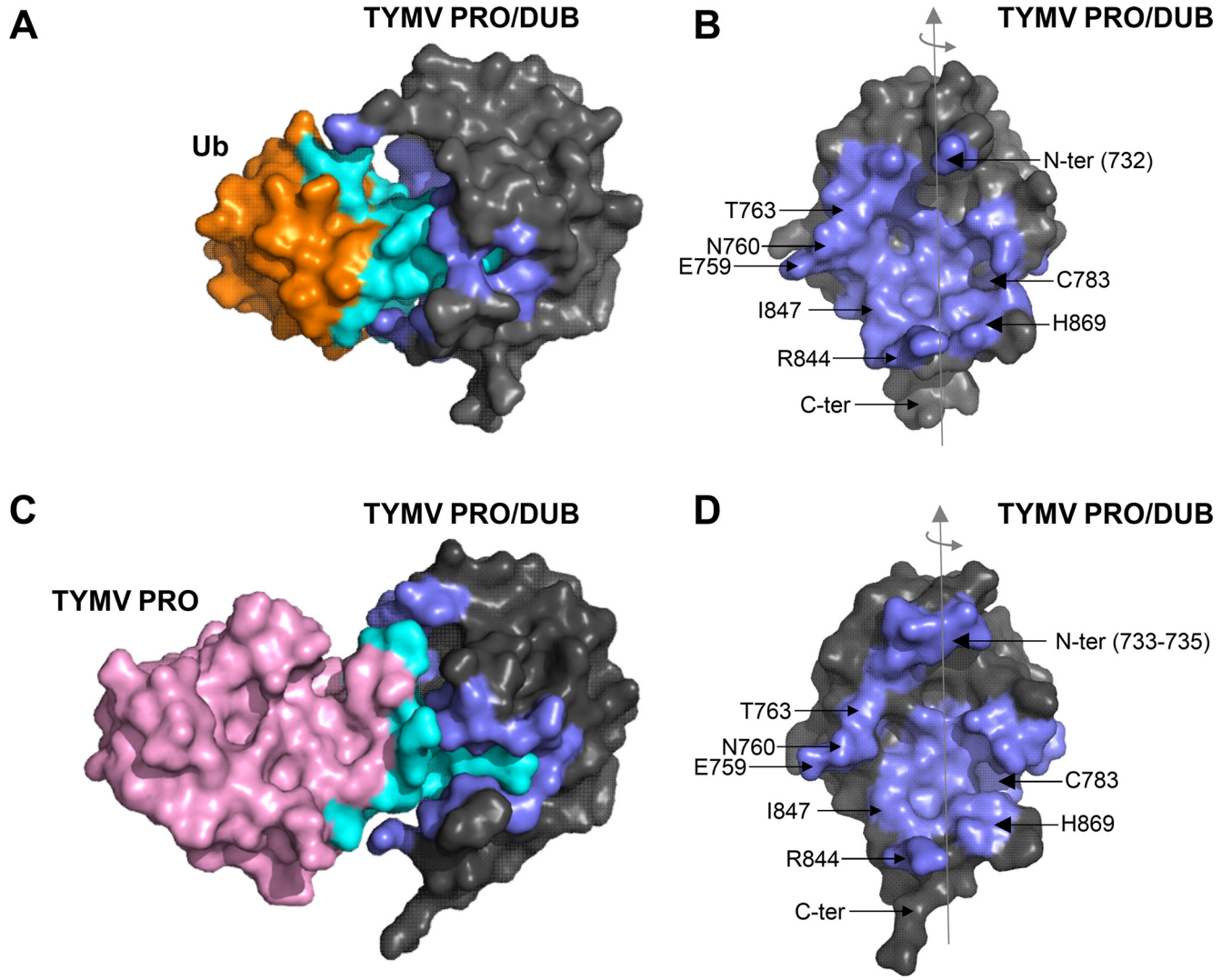

Figure 5. Comparison of the binding interfaces in the PRO/DUB–Ub and PRO/DUB·PRO complexes. *A* and *C*, covalent and noncovalent complexes between TYMV PRO/DUB and Ub (this work) (*A*) or TYMV PRO/DUB from the PRO↓HEL cleavage site (PDB code 4A5U (34)) (*C*), respectively, are shown in surface representation. The enzyme TYMV PRO/DUB is colored in *gray*, and the substrates Ub and TYMV PRO/DUB are colored in *orange* and *pink*, respectively. *B* and *D*, the interacting surfaces used by the enzyme to bind its substrates (*B*, Ub; *D*, PRO/DUB) are colored in *cyan* and are shown after rotation of the protein.

allows (+)ssRNA viruses to ensure numerous enzymatic functions despite a small and compact genome.

TYMV PRO/DUB contacts the bodies of unrelated substrates through highly overlapping recognition patches

By comparing the PRO/DUB–Ub and PRO/DUB·PRO complexes (Fig. 5, *A* and *C*), we show that the TYMV PRO/DUB recognition surfaces for two of its substrates overlap to a large extent (Fig. 5, *B* and *D*). Notably, as for Ub binding (Fig. 5*B*), PRO binding involves residues Glu^{759}-Asn^{760} on one side and Arg^{844} on the other, with Ile^{847} in the middle (Fig. 5*B*). However, the N terminus of TYMV PRO/DUB differently recognizes the substrates. Although the Pro^{733}-Ala^{734}-Pro^{735} motif is prominently involved in PRO recognition (Fig. 5*D*), only Leu^{732} (Fig. 5*B*) makes a tenuous contact to Ub in the crystal structure (Fig. S2), a contact that is not stable in simulations (see above). The Pro^{733}-Ala^{734}-Pro^{735} motif provides a strong additional apolar contact that makes the PRO/DUB·PRO complex less dependent on the hydrophobic bottom of the binding groove. Indeed, our structural data and mutagenesis studies (this work and Refs. 28 and 34) establish Ile^{847} as a central residue for Ub recognition but with less of an impact on PRO binding. In addition, the enzyme harbors a single catalytic site, comprised of Cys^{783} and His^{869}, for both its protease and deubiquitinase activities. PRO and Ub thus share the same TYMV PRO/DUB ligand-binding site and bind in an orientation that exposes their C-terminal extremity toward the catalytic residues. Their interactions with TYMV PRO/DUB are therefore mutually exclusive and compete for binding to the enzyme. This regulates the dual PRO and DUB activities, both in time (proteolytic maturation of the polyprotein at early stages of infection and then regulation of the 66K RdRp amount in later stages) and in space (within the cytoplasm where the polyprotein is translated; then within the viral replication complexes where the viral RNA genome is replicated).

Discussion

Ub is a small molecule that interacts with many very different partners. Despite the wide variety of structural folds and functions encountered in UBPs, Ub interacts with most of them through the same surface(s). In most of the Ub·UBP complexes, Ub engages a canonical protein interaction site known as the "hydrophobic Ile^{44} patch" (6, 52). A second hydrophobic patch of Ub, centered around Ile^{36}, can also be targeted by UBPs (6). Although the Ile^{44} patch is a well-known hot spot used by Ub to interact with its partners, fewer studies report an Ile^{36}-based interface (44, 53). In addition, growing evidence shows the importance of Leu^{8} in UBP binding. Leu^{8} is located between the two hydrophobic patches and is usually considered to be part of the Ile^{44} patch (6, 52). However, Leu^{8} is located in a flexible loop that can undergo conformational changes (42, 43), shifting from a "loop-out" to a "loop-in" conformation (44). In turn, Leu^{8} can be displaced from the Ile^{44} patch to become a component of the Ile^{36} patch (44).

An unusual mode of ubiquitin binding

In TYMV PRO/DUB–Ub complex, Ub engages not only both of its two hydrophobic patches simultaneously but also the loop that comprises Leu^{8} (Fig. 2), a mode of binding without precedent thus far (see below). To score the relative importance of the residues interacting with the two hydrophobic patches, we designed and assayed nonconservative TYMV PRO/DUB mutations aimed at disrupting the binding interface. Mutation of residues that interact with Ile^{44} patch (E759A, N760A, and T763A) had a mild effect on DUB activity (Fig. 3*A*), probably because of their contribution in Ub recognition. Altering the central residue (mutation R844A; Fig. 3*A*) in the interaction of TYMV PRO/DUB with Ub Ile^{36} patch dramatically improved DUB activity, a result that likely reflects improved Ub binding, as confirmed by molecular dynamics simulations. This binding interface thus appears far from optimal for ubiquitin binding. Regarding the motif that interacts with Ub Ile^{8}, we had previously shown the critical role played by TYMV PRO/DUB Ile^{847} in Ub recognition (28, 34). The crystal structure of the TYMV PRO/DUB–Ub complex presented here establishes that Ile^{847} and Phe^{849} engage in strong hydrophobic contacts with Ub Leu^{8} and Thr^{9} from the flexible loop (Fig. 2*G*). In addition, this loop adopts a position where Leu^{8} no longer belongs to any hydrophobic patch but instead forms a distinct hydrophobic motif (Fig. 2, *G* and *H*). Altogether, our results show that the primary determinant of the TYMV PRO/DUB·Ub interaction is centered neither around Ile^{44} as usually observed nor around the Ile^{36} patch. Instead, Leu^{8}, located between the two hydrophobic patches, directly interacts with TYMV PRO/DUB Ile^{847}, located between the two polar patches that sense the Ub patches. The Leu^{8}:Ile^{847} pair therefore makes the major contribution to this interaction. Leu^{8} could thus be a major determinant in Ub involved in sensing its partners (43, 44, 54).

It is interesting to compare how Ub binds to different viral DUBs, including those that have the dual PRO and DUB activities. The other viral OTU DUBs for which the structures of complexes with Ub are available are encoded by Crimean-Congo hemorrhagic fever orthonairovirus (CCHFV) (55), Dugbe virus (DUGV) (56), and Equine arteritis virus (EAV) (25). The EAV PLP2 is an interesting case. It is an OTU PRO/DUB like TYMV's. Furthermore EAV belongs to the order *Nidovirales* that also includes coronaviruses, members of which have caused three deadly epidemics in the 21st century including the current COVID-19 pandemic (57). All *Nidovirales* encode several proteases, at least one of which is a papain-like protease that doubles up as a DUB (58). However, in coronaviruses this PRO/DUB does not belong to the OTU family as in EAV, but to the ubiquitin-specific protease (USP) family (7). This illustrates the capability of RNA viruses to acquire multiple cellular genes for the same function. It also underlines the major argument in favor of the view that TYMV PRO/DUB is a modified cellular DUB that secondarily acquired its processing protease function: it belongs to a family (OTU) of strict DUBs with no PRO activity, the only exceptions being a few viral OTU DUBs with dual PRO/DUB activity. We include in our structural comparison the USP PRO/DUBs encoded by the coronaviruses SARS-CoV (41), MERS-CoV (59), and MHV (PDB 5WFI).[5] The comparison is also extended to cellular DUBs of the OTU family. We use cellular OTU DUBs from yeast (60) and human (61). The mode of interaction of Ub with TYMV PRO/DUB is thus seen to be very divergent. In all cases, other viral DUBs interact with the body of Ub only through its Ile^{44} patch (Fig. 6). The Leu^{8} loop of Ub is most often found in the "loop-out" conformation (Fig. 6, *insets*), Leu^{8} being consequently part of Ile^{44} patch, including for cellular OTU DUBs. In the viral complexes with MHV PLP2, EAV PLP2 or CCHFV vOTU, the Ub Leu^{8} loop occupies the intermediate position observed in TYMV PRO/DUB–Ub complex (Fig. 6, *insets*). The loop adopts this intermediate position in all other crystal structures of complexes involving CCHFV vOTU and Ub (62, 63) (data not shown). These comparisons show that Ub Leu^{8} usually belongs to the Ile^{44} patch but also can be located between the two Ub hydrophobic patches to contact its partner. This intermediate position is found regardless of the enzyme considered, *i.e.* either a dual PRO/DUB or a DUB, either of viral or of cellular origin. Therefore, the function of Leu^{8} is not a hallmark of a DUB family but a specific feature of some enzymes, such as TYMV PRO/DUB.

Superimpositions of TYMV PRO/DUB with cellular OTU DUBs show that yeast OTU1 and human OTUD2 also interact simultaneously with the two hydrophobic patches of Ub (Fig. S3*A*) but engage mainly hydrophobic residues, together with one charged residue that structurally resembles Arg^{844} of TYMV PRO/DUB, *i.e.* Glu^{203} in yOTU1 or Arg^{245} in hOTUD2 (Fig. S3). From an evolutionary point of view, TYMV PRO/DUB appears to be a cellular OTU DUB that has acquired a PRO function by retaining the clamp that holds Ub but losing important hydrophobic residues that interact with the two hydrophobic patches of Ub. This produces an enzyme with low DUB activity.

The low DUB activity of TYMV PRO/DUB may be an evolutionary compromise that ensures proper viral replication

TYMV PRO/DUB exhibits a significant but low deubiquitinase activity, its catalytic efficiency k_{app} (which approximates

[5] Mesecar, A.D. & Chen, Y., unpublished.

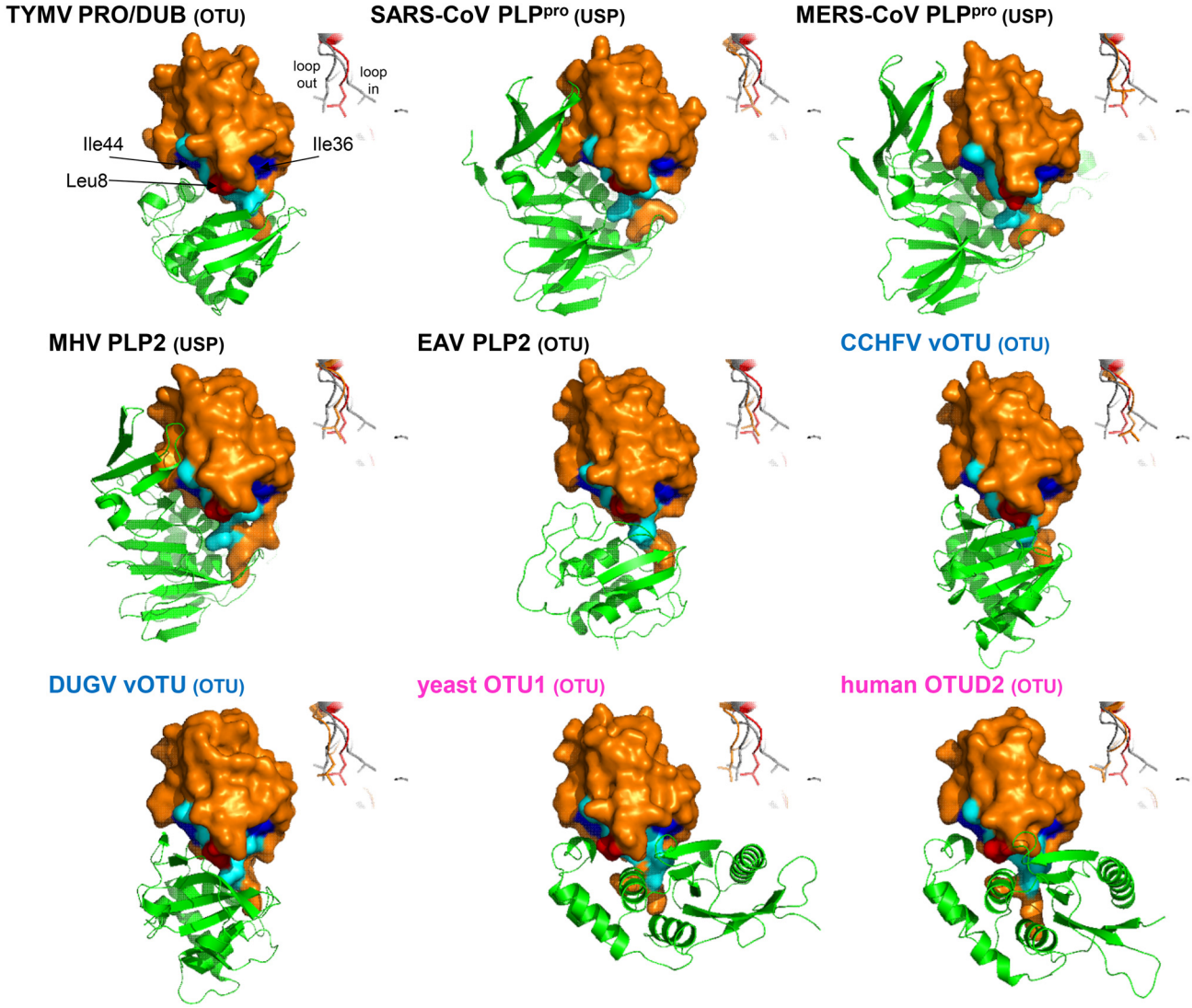

Figure 6. Ub-binding mode with TYMV PRO/DUB and other viral and cellular DUBs. Comparison of overall Ub-binding mode for viral PRO/DUBs (*black lettering*), viral OTU DUBs (*blue lettering*), and cellular OTU DUBs (*magenta lettering*). Whether each enzyme belongs to the OTU or USP family is indicated. Crystal structures of Ub in complex with viral or cellular PRO/DUBs or DUBs were aligned with PyMOL. In each case, Ub is displayed as molecular surface and colored in *orange*, whereas the enzyme is shown in *green* cartoon. The two hydrophobic patches of Ub are colored in *cyan*. Ile^{44} and Ile^{36} of Ub, at the center of the two patches, are shown in *blue*, and Leu^{8}, located in a loop between the two patches, is highlighted in *red*. The conformation of the Ub Leu^{8} loop in each complex is compared with the classical loop-out and loop-in conformations and to the intermediate conformation found in TYMV PRO/DUB–Ub complex (*inset*, see also Fig. 2*G*). We chose for comparison PRO/DUBs encoded by SARS-CoV (PDB code 4MM3 (41)), MERS-CoV (PDB code 4RF1 (59)), MHV (PDB code 5WFI, unpublished structure), and EAV (PDB code 4IUM (25)) (*black*) and DUBs encoded by CCHFV (PDB code 3PHW (55)) and DUGV (PDB code 4HXD (56)) (*blue*). We also compared DUBs from yeast (PDB code 3BY4 (60)) and human (PDB code 4BOS (61)) (*magenta*).

k_{cat}/K_m) being $\sim 2.5 \times 10^3$ M^{-1} s^{-1} (24, 28, 34), which is 10–1,000-fold lower than that of other DUBs such as CCHFV vOTU, EAV PLP2, or MERS-CoV or SARS-CoV PL^{pro} (25, 55, 56, 64). Several nonmutually exclusive hypotheses can be proposed that explain this low activity.

First, the crystal structure of TYMV PRO/DUB showed that the protein structurally belongs to the OTU superfamily of DUBs but displays a peculiar active site. Indeed, TYMV PRO/DUB has no Asp or Asn that are usually part of the catalytic triad of OTU DUBs in combination with a Cys and a His, nor any oxyanion hole to stabilize the thioester intermediate of the catalytic mechanism (34). This results in an altered active site and explains the low DUB activity. In some cases, one or several catalytic functional groups are provided by the substrate, restoring a functional active site, a phenomenon called substrate-assisted catalysis (65). The crystal structure of the TYMV PRO/DUB–Ub complex presented in this work shows that Ub does not supply any residue that would restore a complete DUB active site. However, because Ub is located in the P side of TYMV PRO/DUB, it cannot be ruled out that the third residue may be provided by the substrate positioned in the P′ side of the enzyme, *i.e.* the polyubiquitinated polymerase.

Second, the TYMV DUB activity is measured *in vitro* with a recombinant PRO/DUB domain and a single Ub molecule, whereas *in vivo* the enzyme is present in large macromolecular assemblies. Many deubiquitinases possess additional domains, built around a structurally conserved DUB scaffold, that are involved in substrate specificity and regulation of DUB activity. Additional protein domains of the TYMV replication protein may interact with the PRO/DUB domain and/or with its

substrate and thus contribute to the regulation of TYMV DUB activity. DUB activity *in vivo* is in fact carried by the 98K protein (24), a large multidomain protein that comprises both the MT and PRO/DUB domains, separated by a region harboring the chloroplast-targeting domain (66) and a proline-rich region. This domain organization is similar to that found in the C-terminal part of nsP2 protein of numerous alphaviruses. This consists of an N-terminal protease subdomain (nsP2pro) and a C-terminal subdomain with a methyltransferase fold (MT-like), connected by a long loop. Crystal structures of the C-terminal part of nsP2 protein of *Chikungunya virus* (*CHIKV*) and *Venezuelan equine encephalitis virus* (*VEEV*) show several intramolecular interactions between the two subdomains and the involvement of the MT-like subdomain in nsP2pro function (51, 67, 68). Indeed, the nsP2pro active site is located at the interface between the two subdomains, and its accessibility is regulated by the interdomain loop. Moreover, the MT-like subdomain actively participates in nsP2pro's substrate recognition and binding. Although the nsP2pro subdomains of CHIKV and VEEV do not display DUB activity, these findings illustrate the opportunities for protease regulation inherent to the inclusion of the TYMV PRO/DUB domain in a larger protein. Crystal structures comprising full-length polyubiquitinated 66K and/or 98K protein should help to understand the role of the substrate and/or the other domains of 98K protein in TYMV DUB activity.

Third, Arg^{844} may contribute to the protease activities of TYMV PRO/DUB because it forms a minor contact to the substrate in the PRO/DUB·PRO complex (Fig. 5, *C* and *D*). Analyses of the PRO↓HEL and HEL↓POL cleavages *in vivo* indicate that processing of the polyprotein is not affected by the R844A mutation (Fig. S5). However, we cannot rule out that proteolytic activity also occurs on presently unknown cellular substrates, as with other viral proteases. In such a case, the presence of the nonoptimal Arg^{844} to contact Ub could be a tradeoff to bind efficiently other substrates with unrelated surfaces.

Fourth, and this is our preferred hypothesis in view of the lack of discernible effect on processing protease activity of R844A, low DUB activity may be a fine-tuned feature of TYMV PRO/DUB. Indeed, viral proteases are usually highly specific enzymes whose activity depends not only on the particular sequence of a cleavage site but also on the remainder of the substrate. The cleavage site, often located in a solvent-exposed flexible loop, is commonly recognized by proteases in an extended conformation that favors its perfect positioning into the catalytic cleft (69). Substrate specificity is ensured by specific interactions between the body of the substrate and the enzyme. Although Ub is usually recognized through its Ile^{44} hydrophobic patch only (6, 52), we show in this work that TYMV PRO/DUB, unlike other viral PRO/DUBs, has maintained the cellular OTU DUB mode of recognition, involving the two hydrophobic patches on Ub simultaneously. Nevertheless, the interacting surface is both small and suboptimal in its composition, as shown by mutants that improve the DUB activity (Fig. 3*A*). Because recognition of the substrate body is usually the driving force that allows enzyme/substrate recognition, this observation is puzzling. Residues involved in Ub recognition are not conserved in the *Tymoviridae* family (Fig. 1*B* and Fig. S4). We hypothesize that maintaining a low DUB activity may be an evolutionary compromise to ensure proper viral replication. Indeed, although it is initially produced in amounts equimolar to 98K and 42K (the two other products of the 206K polyprotein maturation process), 66K displays a transient accumulation in the viral replication cycle (33). The 66K polypeptide is degraded at a late stage of viral infection by the ubiquitin proteasome system through polyubiquitination (14). Nevertheless, by harboring a DUB activity, TYMV possesses a rescue system to avoid complete degradation of the 66K protein. This ensures maintenance of the appropriate level of polymerase and safeguards efficient replication of the TYMV genome. This level may be reached with low DUB activity. In the case of TYMV, too high a level of 66K is actually detrimental to replication. We suggest that a finely tuned DUB activity may be a general feature of viruses that use deubiquitination to adjust the amount of protein(s) that is/are critical for their replication. Indeed, Lei and Hilgenfeld (40) found that the MERS-CoV PL^{pro} Ub-binding surface is likewise suboptimal and nicely discussed the functional implications of this finding. Future experiments will be aimed at determining whether this applies also to the case of TYMV.

Materials and methods

Covalent coupling of Ub to TYMV PRO/DUB

TYMV recombinant PRO/DUB fused to an N-terminal His_6 tag (34) was expressed and purified as previously described (28), and diluted to a final concentration of 5 mg/ml in a fresh buffer composed of 10 mM Tris-HCl, 350 mM ammonium acetate, 1 mM DTT, pH 8. A C-terminally modified vinyl methyl ester variant of HA-tagged ubiquitin (HA–Ub-VME) was prepared in 50 mM sodium acetate, pH 4.5, essentially as previously described (36). To adjust the pH, HA–Ub-VME was then diluted 10-fold in binding buffer (50 mM Tris-HCl, 150 mM NaCl, pH 8) and incubated for 10 min at 25 °C. Conjugation of both proteins was achieved by adding a 2-fold molar excess of His_6–PRO/DUB to HA–Ub-VME followed by incubation at 25 °C for 30 min. Unreacted proteins were removed by size-exclusion chromatography on a HiLoad 16/600 Superdex 75-pg column (GE Healthcare) with 50 mM Tris-HCl, 500 mM NaCl, pH 8, as elution buffer. Elution fractions were verified by 16.5% Tris-Tricine SDS-PAGE, and those containing pure 6His-PRO/DUB-HA-Ub complex were pooled and dialyzed overnight at 4 °C against binding buffer. Covalent complex was then concentrated to 24 mg/ml using ultrafiltration on Amicon Ultra with a cutoff of 10 kDa and frozen in liquid nitrogen for storage at −80 °C.

Crystallization of His_6–PRO/DUB–HA–Ub complex

Crystallization conditions of His_6–PRO/DUB–HA–Ub complex were screened by a robot using commercial kits from QIAgen and the sitting-drop vapor-diffusion method. Some promising conditions were manually reproduced at 19 °C in larger drop volumes (1 μl of 15 mg/ml complex solution plus 1 μl of crystallization reagent equilibrated against a 0.5-ml reservoir volume) using the hanging-drop vapor-diffusion setup. Few

crystals appeared after several months in 20% PEG-20K, 0.1 M MES-NaOH, pH 6.5. Prior to data collection, these crystals were harvested, transferred to a cryo-protectant solution (21% PEG-20K, 0.1 M MES-NaOH, pH 6.5, 20% glycerol), and flash-frozen in liquid nitrogen.

Data collection and processing and structure determination

Data collection was performed at Beamline PROXIMA-1 at French synchrotron SOLEIL. Only one crystal showed correct diffraction, and a complete data set could be collected at 3.66 Å. The data were processed and scaled with XDS (70). Because structures of individual TYMV PRO/DUB and human ubiquitin were available, the structure of the His_6-PRO/DUB–HA–Ub complex was solved by molecular replacement. Calculation of the Matthews coefficient (71) suggested two complex molecules in the asymmetric unit, and several molecular replacement protocols were tested with Phaser (72). The good solution consisted of first locating one complex molecule using a C-terminally truncated version of TYMV PRO/DUB (PDB code 5LW5 chain A (28)) and ubiquitin (PDB code 1UBQ (73)) as search models and second using the resulting solution as an input to find the second complex molecule. The electron density was of sufficient quality to manually rebuild the model in COOT (74). Initial stages of refinement were done with REFMAC (75) and then with PHENIX (76). Because of the low resolution, no solvent molecules could be modeled. The final model thus consists of two TYMV PRO/DUB molecules (residues 732–876 in chain A and residues 732–876 in chain C; His tags could not be modeled) and two HA–Ub-VME molecules (residues 1–76 in chain B and residues 1–76 in chain D; HA tags could not be modeled). The data processing and refinement statistics are listed in Table 1.

Molecular dynamics simulations and structure visualization

Molecular dynamics simulations of a TYMV PRO/DUB·Ub product state complex and of a R844A mutant thereof were performed using the AMBER16 program suite (77) with the ff14SB force field. We noted in preliminary simulations comprising residues 732–876 of PRO/DUB that the first residues tended to interact with Ub, but this seemed to be influenced by the +1 charge spuriously added to Leu^{732} by taking it as the N terminus. Thus, we simulated a complex made of an *N*-acetylated PRO/DUB 727–876 (residues 727–731 were modeled stereochemically) and all ubiquitin residues (1–76). The LEaP program was used for preparation of the systems. Hydrogen atoms were added with default parameters. The complexes were neutralized with K^+ cations and immersed in an explicit TIP3P water box with a solvation shell at least 12 Å deep. The systems were then minimized and used to initiate molecular dynamics. All simulations were performed in the isothermal isobaric ensemble (p = 1 atm, T = 300 K), regulated with the Berendsen barostat and thermostat (78), using periodic boundary conditions and Ewald sums for treating long range electrostatic interactions (79). The hydrogen atoms were constrained to the equilibrium bond length using the SHAKE algorithm (80). A 2-fs time step for the integration of Newton's equations was used. The nonbonded cutoff radius of 10 Å was used. All simulations were run with the SANDER module of the AMBER package. Each complex was simulated for 50 ns twice, and the trajectories were sampled every 10 ps. Analysis of the trajectories with cpptraj showed convergence within the first 5 ns as judged by stabilization of root-mean square deviation. The last 45 ns were kept for analyses.

All simulation trajectories and crystal structures were visualized and structural figures were made with PyMOL (81). PyMOL was also used to mutate Arg^{844} to Ala prior to system preparation.

Deubiquitination assay in vitro

Point mutations were introduced in the bacterial vector encoding TYMV PRO/DUB (34) by using the QuikChange II site-directed mutagenesis (Agilent) strategy. Recombinant PRO/DUB proteins were produced and purified as described previously (34). Prior to deubiquitination assay, the purified proteins were dialyzed overnight at 4 °C in buffer 50 mM HEPES-KOH, 150 mM KCl, 1 mM DTT, 10% glycerol, pH 8.0, adjusted to a concentration of 100 μM and kept at −80 °C until use. The fluorogenic substrate Ub-AMC (Boston Biochem) dissolved in DMSO was diluted in assay buffer (50 mM HEPES-KOH, 10 mM KCl, 0.5 mM EDTA, 5 mM DTT, 0.5% Nonidet P-40, pH 7.8). DUB activity was assessed at room temperature in a Hitachi F2000 spectrofluorometer in assay buffer with a final concentration of DMSO adjusted to 2% to match the DMSO concentration in the highest Ub-AMC concentration assays. Reactions were initiated by the addition of enzyme to the cuvette, and the rate of substrate hydrolysis was determined by monitoring AMC-released fluorescence at 440 nm (excitation at 380 nm) for 10 min. Enzyme concentrations were 125 nM for WT PRO/DUB and mutants. To determine the apparent k_{cat}/K_m (K_{app}), the substrate concentration was kept at a concentration below 0.5 μM with the initial velocity linear in substrate concentration, and K_{app} values were then determined according to the equation $V/[E] = K_{app}/[S]$ as described previously (24). Depending on the batch of Ub-AMC, the DUB activity of the WT enzyme displayed variability, with K_{app} varying between 2,388 ± 398 and 2,824 ± 213 M^{-1} s^{-1}. Hence, the activity of the WT protein was measured as a reference for each independent experiment, and the K_{app} values of mutant proteins were normalized to that of the WT protein measured simultaneously. All experiments were performed at least in duplicate, and the data are expressed as the means and standard deviations of these independent experiments.

Data availability

The structure presented in this article has been deposited in the Protein Data Bank with the following code: 6YPT. All remaining data are contained within the article.

Acknowledgments—We are grateful to Jean-Baptiste Charbonnier, Audrey Comte and Cédric Montigny for assistance with equipment for protein purification. We thank Beamline PROXIMA-1 at SOLEIL Synchrotron for generous allocation of beam time and gratefully acknowledge Léonard Chavas's help in data collection and processing.

We acknowledge the help from the staff of the Institute for Integrative Biology of the Cell computing facility Service Informatique et Calcul Scientifique (SICS) for the molecular dynamics simulations.

Author contributions—S. F., I. J., and S. B. conceptualization; S. F., M. A., I. J., and S. B. investigations; S. F., I. J., and S. B. methodology; S. F. and S. B. writing-original draft; S. F., M. A., H. L. P., I. J., and S. B. writing-review and editing; M. D. W., C. S. T., and H. L. P. resources; I. J. and S. B. funding acquisition.

Funding and additional information—This work has benefited from the Core Institute for Integrative Biology of the Cell crystallization platform, supported by French Infrastructure for Integrated Structural Biology Grant ANR-10-INSB-05-01. This work and M. A. were supported by the Agence Nationale de la Recherche Contracts ANR-11-BSV8-011 "Ubi-or-not-ubi" and ANR-16-CE20-0015 "ViroDUB."

Conflict of interest— The authors declare that they have no conflicts of interest with the contents of this article.

Abbreviations—The abbreviations used are: Ub, ubiquitin; DUB, deubiquitinase; PRO, protease; RdRp, RNA-dependent RNA polymerase; TYMV, Turnip yellow mosaic virus; MT, methyltransferase; HEL, helicase; POL, polymerase; OTU, ovarian tumor; VME, vinyl methylester; UBP, ubiquitin-binding protein; AMC, 7-amino-4-methyl coumarin; USP, ubiquitin-specific protease; SARS, Severe acute respiratory syndrome; CoV, coronavirus; MERS, Middle East respiratory syndrome; MHV, Murine hepatitis virus; PDB, Protein Data Bank; CCHFV, Crimean-Congo hemorrhagic fever orthonairovirus; DUGV, Dugbe virus; EAV, Equine arteritis virus.

References

1. Alcaide-Loridan, C., and Jupin, I. (2012) Ubiquitin and plant viruses, let's play together! *Plant Physiol.* **160,** 72–82 CrossRef Medline
2. Gustin, J. K., Moses, A. V., Früh, K., and Douglas, J. L. (2011) Viral takeover of the host ubiquitin system. *Front. Microbiol.* **2,** 161 CrossRef Medline
3. Isaacson, M. K., and Ploegh, H. L. (2009) Ubiquitination, ubiquitin-like modifiers, and deubiquitination in viral infection. *Cell Host Microbe* **5,** 559–570 CrossRef Medline
4. Luo, H. (2016) Interplay between the virus and the ubiquitin-proteasome system: molecular mechanism of viral pathogenesis. *Curr. Opin. Virol.* **17,** 1–10 CrossRef Medline
5. Viswanathan, K., Früh, K., and DeFilippis, V. (2010) Viral hijacking of the host ubiquitin system to evade interferon responses. *Curr. Opin. Microbiol.* **13,** 517–523 CrossRef Medline
6. Komander, D., and Rape, M. (2012) The ubiquitin code. *Annu. Rev. Biochem.* **81,** 203–229 CrossRef Medline
7. Komander, D., Clague, M. J., and Urbé, S. (2009) Breaking the chains: structure and function of the deubiquitinases. *Nat. Rev. Mol. Cell Biol.* **10,** 550–563 CrossRef
8. Clague, M. J., and Urbé, S. (2010) Ubiquitin: same molecule, different degradation pathways. *Cell* **143,** 682–685 CrossRef Medline
9. Choi, A. G., Wong, J., Marchant, D., and Luo, H. (2013) The ubiquitin-proteasome system in positive-strand RNA virus infection. *Rev. Med. Virol.* **23,** 85–96 CrossRef Medline
10. Randow, F., and Lehner, P. J. (2009) Viral avoidance and exploitation of the ubiquitin system. *Nat. Cell Biol.* **11,** 527–534 CrossRef Medline
11. Bailey-Elkin, B. A., Knaap, R. C. M., Kikkert, M., and Mark, B. L. (2017) Structure and function of viral deubiquitinating enzymes. *J. Mol. Biol.* **429,** 3441–3470 CrossRef Medline
12. Wimmer, P., and Schreiner, S. (2015) Viral mimicry to usurp ubiquitin and SUMO host pathways. *Viruses* **7,** 4854–4872 CrossRef Medline
13. Zhao, C., Collins, M. N., Hsiang, T.-Y., and Krug, R. M. (2013) Interferon-induced ISG15 pathway: an ongoing virus–host battle. *Trends Microbiol.* **21,** 181–186 CrossRef Medline
14. Camborde, L., Planchais, S., Tournier, V., Jakubiec, A., Drugeon, G., Lacassagne, E., Pflieger, S., Chenon, M., and Jupin, I. (2010) The ubiquitin-proteasome system regulates the accumulation of Turnip yellow mosaic virus RNA-dependent RNA polymerase during viral infection. *Plant Cell* **22,** 3142–3152 CrossRef Medline
15. Kerkvliet, J., Papke, L., and Rodriguez, M. (2011) Antiviral effects of a transgenic RNA-dependent RNA polymerase. *J. Virol.* **85,** 621–625 CrossRef Medline
16. de Groot, R. J., Rümenapf, T., Kuhn, R. J., Strauss, E. G., and Strauss, J. H. (1991) Sindbis virus RNA polymerase is degraded by the N-end rule pathway. *Proc. Natl. Acad. Sci. U.S.A.* **88,** 8967–8971 CrossRef Medline
17. Héricourt, F., Blanc, S., Redeker, V., and Jupin, I. (2000) Evidence for phosphorylation and ubiquitinylation of the turnip yellow mosaic virus RNA-dependent RNA polymerase domain expressed in a baculovirus-insect cell system. *Biochem. J.* **349,** 417–425 CrossRef Medline
18. Losick, V. P., Schlax, P. E., Emmons, R. A., and Lawson, T. G. (2003) Signals in hepatitis A virus P3 region proteins recognized by the ubiquitin-mediated proteolytic system. *Virology* **309,** 306–319 CrossRef Medline
19. Abdul Rehman, S. A., Kristariyanto, Y. A., Choi, S.-Y., Nkosi, P. J., Weidlich, S., Labib, K., Hofmann, K., and Kulathu, Y. (2016) MINDY-1 is a member of an evolutionarily conserved and structurally distinct new family of deubiquitinating enzymes. *Mol. Cell* **63,** 146–155 CrossRef Medline
20. Hermanns, T., Pichlo, C., Woiwode, I., Klopffleisch, K., Witting, K. F., Ovaa, H., Baumann, U., and Hofmann, K. (2018) A family of unconventional deubiquitinases with modular chain specificity determinants. *Nat. Commun.* **9,** 799 CrossRef Medline
21. Mevissen, T. E. T., and Komander, D. (2017) Mechanisms of deubiquitinase specificity and regulation. *Annu. Rev. Biochem.* **86,** 159–192 CrossRef Medline
22. Barretto, N., Jukneliene, D., Ratia, K., Chen, Z., Mesecar, A. D., and Baker, S. C. (2005) The papain-like protease of severe acute respiratory syndrome coronavirus has deubiquitinating activity. *J. Virol.* **79,** 15189–15198 CrossRef Medline
23. Békés, M., Rut, W., Kasperkiewicz, P., Mulder, M. P. C., Ovaa, H., Drag, M., Lima, C. D., and Huang, T. T. (2015) SARS hCoV papain-like protease is a unique Lys^{48} linkage-specific di-distributive deubiquitinating enzyme. *Biochem. J.* **468,** 215–226 CrossRef Medline
24. Chenon, M., Camborde, L., Cheminant, S., and Jupin, I. (2012) A viral deubiquitylating enzyme targets viral RNA-dependent RNA polymerase and affects viral infectivity. *EMBO J.* **31,** 741–753 CrossRef Medline
25. van Kasteren, P. B., Bailey-Elkin, B. A., James, T. W., Ninaber, D. K., Beugeling, C., Khajehpour, M., Snijder, E. J., Mark, B. L., and Kikkert, M. (2013) Deubiquitinase function of arterivirus papain-like protease 2 suppresses the innate immune response in infected host cells. *Proc. Natl. Acad. Sci. U.S.A.* **110,** E838–E847 CrossRef Medline
26. Lindner, H. A., Fotouhi-Ardakani, N., Lytvyn, V., Lachance, P., Sulea, T., and Ménard, R. (2005) The papain-like protease from the severe acute respiratory syndrome coronavirus is a deubiquitinating enzyme. *J. Virol.* **79,** 15199–15208 CrossRef Medline
27. Wang, D., Fang, L., Li, P., Sun, L., Fan, J., Zhang, Q., Luo, R., Liu, X., Li, K., Chen, H., Chen, Z., and Xiao, S. (2011) The leader proteinase of foot-and-mouth disease virus negatively regulates the type I interferon pathway by acting as a viral deubiquitinase. *J. Virol.* **85,** 3758–3766 CrossRef Medline
28. Jupin, I., Ayach, M., Jomat, L., Fieulaine, S., and Bressanelli, S. (2017) A mobile loop near the active site acts as a switch between the dual activities of a viral protease/deubiquitinase. *PLoS Pathog.* **13,** e1006714 CrossRef Medline
29. Bransom, K. L., Wallace, S. E., and Dreher, T. W. (1996) Identification of the cleavage site recognized by the turnip yellow mosaic virus protease. *Virology* **217,** 404–406 CrossRef Medline
30. Jakubiec, A., Drugeon, G., Camborde, L., and Jupin, I. (2007) Proteolytic processing of turnip yellow mosaic virus replication proteins and functional impact on infectivity. *J. Virol.* **81,** 11402–11412 CrossRef Medline

31. Kadaré, G., Rozanov, M., and Haenni, A. L. (1995) Expression of the turnip yellow mosaic virus proteinase in *Escherichia coli* and determination of the cleavage site within the 206 kDa protein. *J. Gen. Virol.* **76,** 2853–2857 CrossRef Medline
32. Jakubiec, A., Tournier, V., Drugeon, G., Pflieger, S., Camborde, L., Vinh, J., Héricourt, F., Redeker, V., and Jupin, I. (2006) Phosphorylation of viral RNA-dependent RNA polymerase and its role in replication of a plus-strand RNA virus. *J. Biol. Chem.* **281,** 21236–21249 CrossRef Medline
33. Prod'homme, D., Le Panse, S., Drugeon, G., and Jupin, I. (2001) Detection and subcellular localization of the turnip yellow mosaic virus 66K replication protein in infected cells. *Virology* **281,** 88–101 CrossRef Medline
34. Lombardi, C., Ayach, M., Beaurepaire, L., Chenon, M., Andreani, J., Guerois, R., Jupin, I., and Bressanelli, S. (2013) A compact viral processing proteinase/ubiquitin hydrolase from the OTU family. *PLoS Pathog.* **9,** e1003560 CrossRef Medline
35. Robin, C., Beaurepaire, L., Chenon, M., Jupin, I., and Bressanelli, S. (2012) In praise of impurity: 30S ribosomal S15 protein-assisted crystallization of turnip yellow mosaic virus proteinase. *Acta Crystallograph. Sect. F Struct. Biol. Cryst. Commun.* **68,** 486–490 CrossRef Medline
36. Borodovsky, A., Ovaa, H., Kolli, N., Gan-Erdene, T., Wilkinson, K. D., Ploegh, H. L., and Kessler, B. M. (2002) Chemistry-based functional proteomics reveals novel members of the deubiquitinating enzyme family. *Chem. Biol.* **9,** 1149–1159 CrossRef Medline
37. Misaghi, S., Galardy, P. J., Meester, W. J. N., Ovaa, H., Ploegh, H. L., and Gaudet, R. (2005) Structure of the ubiquitin hydrolase UCH-L3 complexed with a suicide substrate. *J. Biol. Chem.* **280,** 1512–1520 CrossRef Medline
38. Krissinel, E., and Henrick, K. (2007) Inference of macromolecular assemblies from crystalline state. *J. Mol. Biol.* **372,** 774–797 CrossRef Medline
39. Capodagli, G. C., McKercher, M. A., Baker, E. A., Masters, E. M., Brunzelle, J. S., and Pegan, S. D. (2011) Structural analysis of a viral ovarian tumor domain protease from the Crimean–Congo hemorrhagic fever virus in complex with covalently bonded ubiquitin. *J. Virol.* **85,** 3621–3630 CrossRef Medline
40. Lei, J., and Hilgenfeld, R. (2016) Structural and mutational analysis of the interaction between the Middle-East respiratory syndrome coronavirus (MERS-CoV) papain-like protease and human ubiquitin. *Virol. Sin.* **31,** 288–299 CrossRef Medline
41. Ratia, K., Kilianski, A., Baez-Santos, Y. M., Baker, S. C., and Mesecar, A. (2014) Structural basis for the ubiquitin-linkage specificity and deISGylating activity of SARS-CoV papain-like protease. *PLoS Pathog.* **10,** e1004113 CrossRef Medline
42. Lange, O. F., Lakomek, N.-A., Farès, C., Schröder, G. F., Walter, K. F. A., Becker, S., Meiler, J., Grubmüller, H., Griesinger, C., and de Groot, B. L. (2008) Recognition dynamics up to microseconds revealed from an RDC-derived ubiquitin ensemble in solution. *Science* **320,** 1471–1475 CrossRef Medline
43. Perica, T., and Chothia, C. (2010) Ubiquitin–molecular mechanisms for recognition of different structures. *Curr. Opin. Struct. Biol.* **20,** 367–376 CrossRef Medline
44. Hospenthal, M. K., Freund, S. M. V., and Komander, D. (2013) Assembly, analysis and architecture of atypical ubiquitin chains. *Nat. Struct. Mol. Biol.* **20,** 555–565 CrossRef Medline
45. Virdee, S., Ye, Y., Nguyen, D. P., Komander, D., and Chin, J. W. (2010) Engineered diubiquitin synthesis reveals Lys29-isopeptide specificity of an OTU deubiquitinase. *Nat. Chem. Biol.* **6,** 750–757 CrossRef Medline
46. Artavanis-Tsakonas, K., Weihofen, W. A., Antos, J. M., Coleman, B. I., Comeaux, C. A., Duraisingh, M. T., Gaudet, R., and Ploegh, H. L. (2010) Characterization and structural studies of the *Plasmodium falciparum* ubiquitin and Nedd8 hydrolase UCHL3. *J. Biol. Chem.* **285,** 6857–6866 CrossRef Medline
47. Johnston, S. C., Riddle, S. M., Cohen, R. E., and Hill, C. P. (1999) Structural basis for the specificity of ubiquitin C-terminal hydrolases. *EMBO J.* **18,** 3877–3887 CrossRef Medline
48. Morrow, M. E., Kim, M.-I., Ronau, J. A., Sheedlo, M. J., White, R. R., Chaney, J., Paul, L. N., Lill, M. A., Artavanis-Tsakonas, K., and Das, C. (2013) Stabilization of an unusual salt bridge in ubiquitin by the extra C-terminal domain of the proteasome-associated deubiquitinase UCH37 as a mechanism of its exo specificity. *Biochemistry* **52,** 3564–3578 CrossRef Medline
49. Ye, Y., Akutsu, M., Reyes-Turcu, F., Enchev, R. I., Wilkinson, K. D., and Komander, D. (2011) Polyubiquitin binding and cross-reactivity in the USP domain deubiquitinase USP21. *EMBO Rep.* **12,** 350–357 CrossRef Medline
50. Golubtsov, A., Kääriäinen, L., and Caldentey, J. (2006) Characterization of the cysteine protease domain of Semliki Forest virus replicase protein nsP2 by *in vitro* mutagenesis. *FEBS Lett.* **580,** 1502–1508 CrossRef Medline
51. Russo, A. T., White, M. A., and Watowich, S. J. (2006) The crystal structure of the Venezuelan equine encephalitis alphavirus nsP2 protease. *Structure* **14,** 1449–1458 CrossRef Medline
52. Dikic, I., Wakatsuki, S., and Walters, K. J. (2009) Ubiquitin-binding domains: from structures to functions. *Nat. Rev. Mol. Cell Biol.* **10,** 659–671 CrossRef Medline
53. Winget, J. M., and Mayor, T. (2010) The diversity of ubiquitin recognition: hot spots and varied specificity. *Mol. Cell* **38,** 627–635 CrossRef Medline
54. Cui, G., Benirschke, R. C., Tuan, H.-F., Juranić, N., Macura, S., Botuyan, M. V., and Mer, G. (2010) Structural basis of ubiquitin recognition by translesion synthesis DNA polymerase ι. *Biochemistry* **49,** 10198–10207 CrossRef Medline
55. Akutsu, M., Ye, Y., Virdee, S., Chin, J. W., and Komander, D. (2011) Molecular basis for ubiquitin and ISG15 cross-reactivity in viral ovarian tumor domains. *Proc. Natl. Acad. Sci. U.S.A.* **108,** 2228–2233 CrossRef Medline
56. Capodagli, G. C., Deaton, M. K., Baker, E. A., Lumpkin, R. J., and Pegan, S. D. (2013) Diversity of ubiquitin and ISG15 specificity among nairoviruses' viral ovarian tumor domain proteases. *J. Virol.* **87,** 3815–3827 CrossRef Medline
57. Wu, F., Zhao, S., Yu, B., Chen, Y.-M., Wang, W., Song, Z.-G., Hu, Y., Tao, Z.-W., Tian, J.-H., Pei, Y.-Y., Yuan, M.-L., Zhang, Y.-L., Dai, F.-H., Liu, Y., Wang, Q.-M., *et al.* (2020) A new coronavirus associated with human respiratory disease in China. *Nature* **579,** 265–269 CrossRef Medline
58. Neuman, B. W. (2016) Bioinformatics and functional analyses of coronavirus nonstructural proteins involved in the formation of replicative organelles. *Antiviral Res.* **135,** 97–107 CrossRef Medline
59. Bailey-Elkin, B. A., Knaap, R. C. M., Johnson, G. G., Dalebout, T. J., Ninaber, D. K., van Kasteren, P. B., Bredenbeek, P. J., Snijder, E. J., Kikkert, M., and Mark, B. L. (2014) Crystal structure of the Middle East respiratory syndrome coronavirus (MERS-CoV) papain-like protease bound to ubiquitin facilitates targeted disruption of deubiquitinating activity to demonstrate its role in innate immune suppression. *J. Biol. Chem.* **289,** 34667–34682 CrossRef Medline
60. Messick, T. E., Russell, N. S., Iwata, A. J., Sarachan, K. L., Shiekhattar, R., Shanks, J. R., Reyes-Turcu, F. E., Wilkinson, K. D., and Marmorstein, R. (2008) Structural basis for ubiquitin recognition by the Otu1 ovarian tumor domain protein. *J. Biol. Chem.* **283,** 11038–11049 CrossRef Medline
61. Mevissen, T. E. T., Hospenthal, M. K., Geurink, P. P., Elliott, P. R., Akutsu, M., Arnaudo, N., Ekkebus, R., Kulathu, Y., Wauer, T., El Oualid, F., Freund, S. M. V., Ovaa, H., and Komander, D. (2013) OTU deubiquitinases reveal mechanisms of linkage specificity and enable ubiquitin chain restriction analysis. *Cell* **154,** 169–184 CrossRef Medline
62. Ekkebus, R., van Kasteren, S. I., Kulathu, Y., Scholten, A., Berlin, I., Geurink, P. P., de Jong, A., Goerdayal, S., Neefjes, J., Heck, A. J. R., Komander, D., and Ovaa, H. (2013) On terminal alkynes that can react with active-site cysteine nucleophiles in proteases. *J. Am. Chem. Soc.* **135,** 2867–2870 CrossRef Medline
63. Zhang, W., Bailey-Elkin, B. A., Knaap, R. C. M., Khare, B., Dalebout, T. J., Johnson, G. G., Kasteren, P. B., van, McLeish, N. J., Gu, J., He, W., Kikkert, M., Mark, B. L., and Sidhu, S. S. (2017) Potent and selective inhibition of pathogenic viruses by engineered ubiquitin variants. *PLoS Pathog.* **13,** e1006372 CrossRef Medline
64. Báez-Santos, Y. M., Mielech, A. M., Deng, X., Baker, S., and Mesecar, A. D. (2014) Catalytic function and substrate specificity of the papain-like protease domain of nsp3 from the Middle East respiratory syndrome coronavirus. *J. Virol.* **88,** 12511–12527 CrossRef Medline

65. Dall'Acqua, W., and Carter, P. (2000) Substrate-assisted catalysis: molecular basis and biological significance. *Protein Sci*. **9,** 1–9 Medline
66. Moriceau, L., Jomat, L., Bressanelli, S., Alcaide-Loridan, C., and Jupin, I. (2017) Identification and molecular characterization of the chloroplast targeting domain of turnip yellow mosaic virus replication proteins. *Front. Plant Sci*. **8,** 2138 CrossRef Medline
67. Hu, X., Compton, J. R., Leary, D. H., Olson, M. A., Lee, M. S., Cheung, J., Ye, W., Ferrer, M., Southall, N., Jadhav, A., Morazzani, E. M., Glass, P. J., Marugan, J., and Legler, P. M. (2016) Kinetic, mutational, and structural studies of the Venezuelan equine encephalitis virus nonstructural protein 2 cysteine protease. *Biochemistry* **55,** 3007–3019 CrossRef Medline
68. Narwal, M., Singh, H., Pratap, S., Malik, A., Kuhn, R. J., Kumar, P., and Tomar, S. (2018) Crystal structure of chikungunya virus nsP2 cysteine protease reveals a putative flexible loop blocking its active site. *Int. J. Biol. Macromol*. **116,** 451–462 CrossRef Medline
69. Madala, P. K., Tyndall, J. D. A., Nall, T., and Fairlie, D. P. (2010) Update 1 of: proteases universally recognize beta strands in their active sites. *Chem. Rev*. **110,** PR1–PR31 CrossRef Medline
70. Kabsch, W. (2010) Integration, scaling, space-group assignment and post-refinement. *Acta Crystallogr. D Biol. Crystallogr*. **66,** 133–144 CrossRef Medline
71. Kantardjieff, K. A., and Rupp, B. (2003) Matthews coefficient probabilities: improved estimates for unit cell contents of proteins, DNA, and protein–nucleic acid complex crystals. *Protein Sci*. **12,** 1865–1871 CrossRef Medline
72. McCoy, A. J., Grosse-Kunstleve, R. W., Adams, P. D., Winn, M. D., Storoni, L. C., and Read, R. J. (2007) Phaser crystallographic software. *J. Appl. Crystallogr*. **40,** 658–674 CrossRef Medline
73. Vijay-Kumar, S., Bugg, C. E., and Cook, W. J. (1987) Structure of ubiquitin refined at 1.8 A resolution. *J. Mol. Biol*. **194,** 531–544 CrossRef Medline
74. Emsley, P., Lohkamp, B., Scott, W. G., and Cowtan, K. (2010) Features and development of Coot. *Acta Crystallogr. D Biol. Crystallogr*. **66,** 486–501 CrossRef Medline
75. Murshudov, G. N., Skubák, P., Lebedev, A. A., Pannu, N. S., Steiner, R. A., Nicholls, R. A., Winn, M. D., Long, F., and Vagin, A. A. (2011) REFMAC5 for the refinement of macromolecular crystal structures. *Acta Crystallogr. D Biol. Crystallogr*. **67,** 355–367 CrossRef Medline
76. Adams, P. D., Afonine, P. V., Bunkóczi, G., Chen, V. B., Davis, I. W., Echols, N., Headd, J. J., Hung, L.-W., Kapral, G. J., Grosse-Kunstleve, R. W., McCoy, A. J., Moriarty, N. W., Oeffner, R., Read, R. J., Richardson, D. C., *et al*. (2010) PHENIX: a comprehensive Python-based system for macromolecular structure solution. *Acta Crystallogr. D Biol. Crystallogr*. **66,** 213–221 CrossRef Medline
77. Case, D. A., Cheatham, T. E., 3rd, Darden, T., Gohlke, H., Luo, R., Merz, K. M., Jr., Onufriev, A., Simmerling, C., Wang, B., and Woods, R. J. (2005) The Amber biomolecular simulation programs. *J. Comput. Chem*. **26,** 1668–1688 CrossRef Medline
78. Berendsen, H. J. C., Postma, J. P. M., Gunsteren, W. F., van, DiNola, A., and Haak, J. R. (1984) Molecular dynamics with coupling to an external bath. *J. Chem. Phys*. **81,** 3684–3690 CrossRef
79. Darden, T., York, D., and Pedersen, L. (1993) Particle mesh Ewald: an Ns? log(N) method for Ewald sums in large systems. *J. Chem. Phys*. **98,** 10089–10092 CrossRef
80. Ryckaert, J.-P., Ciccotti, G., and Berendsen, H. J. C. (1977) Numerical integration of the cartesian equations of motion of a system with constraints: molecular dynamics of n-alkanes. *J. Comput. Phys*. **23,** 327–341 CrossRef
81. DeLano, W. L. (2015) The PyMOL Molecular Graphics System, version 1.8, Schroedinger, LLC, New York
82. Deléage, G. (2017) ALIGNSEC: viewing protein secondary structure predictions within large multiple sequence alignments. *Bioinformatics* **33,** 3991–3992 CrossRef Medline
83. Robert, X., and Gouet, P. (2014) Deciphering key features in protein structures with the new ENDscript server. *Nucleic Acids Res*. **42,** W320–W324 CrossRef Medline
84. Reyes-Turcu, F. E., Ventii, K. H., and Wilkinson, K. D. (2009) Regulation and cellular roles of ubiquitin-specific deubiquitinating enzymes. *Annu. Rev. Biochem*. **78,** 363–397 CrossRef Medline

Turnip yellow mosaic virus protease binds ubiquitin suboptimally to fine-tune its deubiquitinase activity

Sonia Fieulaine, Martin D. Witte, Christopher S. Theile, Maya Ayach, Hidde L. Ploegh, Isabelle Jupin and Stéphane Bressanelli

J. Biol. Chem. 2020, 295:13769-13783.
doi: 10.1074/jbc.RA120.014628 originally published online July 30, 2020